UCLouvain

FACULTE DES SCIENCES

Faculté des sciences

Evaluation of safety margins for cone beam CT-based adaptive prostate radiotherapy

Author: **Florian DUPONT**
Supervisors: **David DECHAMBRE, Edmond STERPIN**
Reader: **Guillaume JANSSENS**
Academic year 2022–2023
Master [120] en sciences physiques

Abstract

Purpose/objective

Adaptive radiotherapy is characterized by the use of a daily imaging system, such as CBCT (Cone-Beam Computed Tomography) images to re-optimize the treatment plan before the delivery of each fraction based on the daily anatomy and position of the patient. By systematically re-delineating the Clinical Target Volume (CTV) and adapting the treatment at each fraction, target delineation uncertainty features a random component instead of a pure systematic one in a non-adaptive workflow. The goal of this work is to identify and characterize all sources of errors in CBCT-based adaptive workflow and compute a new relevant PTV (Planning Target Volume) safety margin.

Material/methods

A total of 169 radiotherapy sessions from 10 prostate cancer patients treated on the Varian ETHOS treatment system have been analyzed. For each of them, the CBCT images and the RTSTRUCT file containing the CTV contours were used to compute the systematic and random contributions of, respectively, the intrafraction motion and the delineation errors. For the later, intra-patient and inter-patient variabilities were computed in six directions, by considering the prostate as a rigid, non-rotating volume. By doing so, we were able to directly compare the delineations done by the physicians on daily CBCT images with the initial delineation done on the CT-sim with the help of an MRI, and sort the directions using the polar coordinates of every point of each contour. The computed variabilities were then corrected for the prostate shape variations based on literature data (Deurloo et al. [2005]) and quadratically added to the random and systematic margin contributions, respectively. For machine-specific errors, the daily machine performance checks reports were used to evaluate the setup error and the convolution product of a parabola and a Gaussian function was used to fit the measured dose profile of the beam at 10 cm in water in order to determine the penumbra contribution.

Results

A penumbra of 2.8mm and a systematic setup error of 0.3mm have been measured. The intrafraction motion error had a systematic contribution of 0.8±0.3, 1.7±0.6 and 0.8±0.4mm for the left-right, anteroposterior and cranocaudal directions, respectively, and a random contribution of 1.2, 2.5 and 1.3mm for the same directions. These results were obtained with time intervals ranging from 10 to 40 minutes. Due to an actual treatment time of only less than 5 minutes, a relatively small population of patients and intrafraction errors significantly greater than what can be found in literature (McPartlin et al. [2016]), we made the choice to use literature data for the intrafraction motion error to compute the total margin. Finally, the addition of the systematic and random contributions of the delineation uncertainty gives a total margin of 3.8, 3.7, 3.9, 3.7, 6.4 and 4.8mm in the left, right, anterior, posterior, cranial and caudal directions, respectively, which represents a reduction of 11 to 40% compared to the margins of 4.8, 6.1 and 7.3mm computed with a fully systematic delineation uncertainty of 1.7, 2 and 2.5mm in the LR, AP and CC directions, respectively.

Conclusion

According to our results, the gain offered by the separation of the delineation uncertainty into systematic and random contributions thanks to the adaptive delineation process justify a reduction of the isotropic PTV margin from 7mm to 5mm. It could even be safely lowered down to 4mm in the left, right, anterior and posterior directions.

Acknowledgements

Many people contributed to the realization of this work. And even if all their names are not on the front page, they all deserve my thanks for their help.

I first want to thanks those who actually are on the front page, my supervisors, David Dechambre and Professor Edmond Sterpin, for their availability, the advice and guidance they gave me whenever I needed it, and for all the things they taught me.

I also would like to thank my friends and family for their support, during this work and in general.
Thank you Eléonore for the time you spent reviewing everything and for the numerous discussion we have had over the past year.

Finally, I want to say that it has been a pleasure to work in the radiotherapy department of Saint-Luc, and I would like to thank all the staff for welcoming me during the few months I spent there.

Abbreviations

Abbreviation	Definition
AI	Artificial Intelligence
AP	Anterior-Posterior
CBCT	Cone Beam Computed Tomography
CC	Cranial-Caudal
CCC	Collapse-Cone Convolution
COM	Center Of Mass
CUSL	Cliniques Universitaires Saint-Luc
CT	Computed Tomography
CT-sim	Computed Tomography simulation
CTV	Clinical Target Volume
DMLC	Dynamic MultiLeaf Collimator
FDG-PET	FluoroDeoxyGlucose Positron Emission Tomography
FFF	Flattening Filter-Free

GTV	Gross Tumor Volume
HU	Hounsfield Unit
ICRP	International Commission on Radiological Protection
IGRT	Image Guided RadioTherapy
IMRT	Intensity Modulated RadioTherapy
IT	Information Technology
Linac	Linear accelerator
LR	Left-Right
MLC	MultiLeaf Collimator
MRI	Magnetic Resonance Imaging
MPC	Machine Performance Checks
OAR	Organ At Risk
pQA	Patient-specific Quality Assurance
PSA	Prostate Specific Antigen
PTV	Planning Target Volume
QA	Quality Assurance
TCP	Tumor Control Probability
TPS	Treatment Planning System
VMAT	Volumetric Modulated Arc Therapy

WHO	World Health Organization

Contents

Chapter 1

Introduction

Prostate cancer is the fourth most common cancer in the world, and one of the major cause of death in the male population, especially in the most developed countries [1]. Nowadays, fortunately, this major thread for men's health has a lot of treatment possibilities, the most common of which being radiotherapy. But despite its undeniable benefits for the survival of the patients, radiotherapy still induce several side effects, due to the irradiation of the surrounding organs. One of the reasons for that is the need of irradiating not only the target, but also a planning target volume (PTV) safety margin around it, in order to ensure its coverage despite the uncertainties and errors that could occur during the treatment. To reduce these uncertainties, and therefore the safety margin, a lot of research and technical improvements have been made in the last few decades. One of the latest is called adaptive radiotherapy. This new evolution is characterized by the use of daily imaging system to re-optimize the treatment plan before the delivery of each fraction based on the daily anatomy and position of the patient. Changing the treatment protocol implies to compute new PTV margins adapted to the situation and the system that we use, in order to ensure a proper dose coverage of the tumor while preserving the healthy tissues.

The goal of this work is then to look at the workflow used for the adaptive radiotherapy of the prostate cancer, identify and characterize all sources of errors and compute a new relevant margin based on the acquired data.

This work will be structured in 4 main parts. In the first one, a general reminder about prostate cancer and radiotherapy will be given, followed by an overview of the theoretical concepts behind margin computation in radiotherapy.

The second part covers the methods used to acquire and process the data required to compute each part of the margin. It focuses particularly on the techniques

developed to separate the random and systematic contributions of each uncertainty.

In the third part, the results are presented for every error source, and a general PTV margin is computed based on the acquired data.

Finally, the last chapters include a discussion of the results, with a comparison to what can be found in the literature, followed by a general conclusion.

Chapter 2

Theoretical reminders

2.1 Prostate Cancer

The prostate gland is a male organ, situated in the pelvic region, alongside the bladder, the rectum and the seminal vesicles (see figure 2.1). It is surrounded by the bladder on the top, the rectum on the back, the inferior pubic ramus on front, the elevator ani muscle on the left and right and at the bottom is found the penile bulb. The role of the prostate is to produce some constituents of the seminal fluid expelled during ejaculation. The other constituents are mainly produced by the seminal vesicles, which are two smaller glands situated a little higher than the prostate, between the bladder and the rectum, and by the penile bulb. Those three organs are therefore essential for male fertility.

The prostate cancer is the fourth most common cancer in the world with 1,414,259 new cases in 2020, behind breast, lung and colorectum according to the World Health Organization (WHO) and the second one in the male population neck and neck with lung cancer [1]. The pathology is usually characterised by the presence of hard nodules in the prostate gland that may be detected during a rectal examination by a proctologist, but are rarely visible by x-ray imaging. Another way to detect the prostate cancer is by performing a blood test to measure the Prostate Specific Antigen (PSA) level, but the only way to confirm the diagnostic is the biopsy, that is taking a sample of the prostate for analysis.

It can be treated by different means, like prostate ablation, chemotherapy, hormonotherapy, brachytherapy, external radiotherapy or a combination of these different treatments. The result is a very good 5-years relative survival rate of 98% in the USA for example [1].

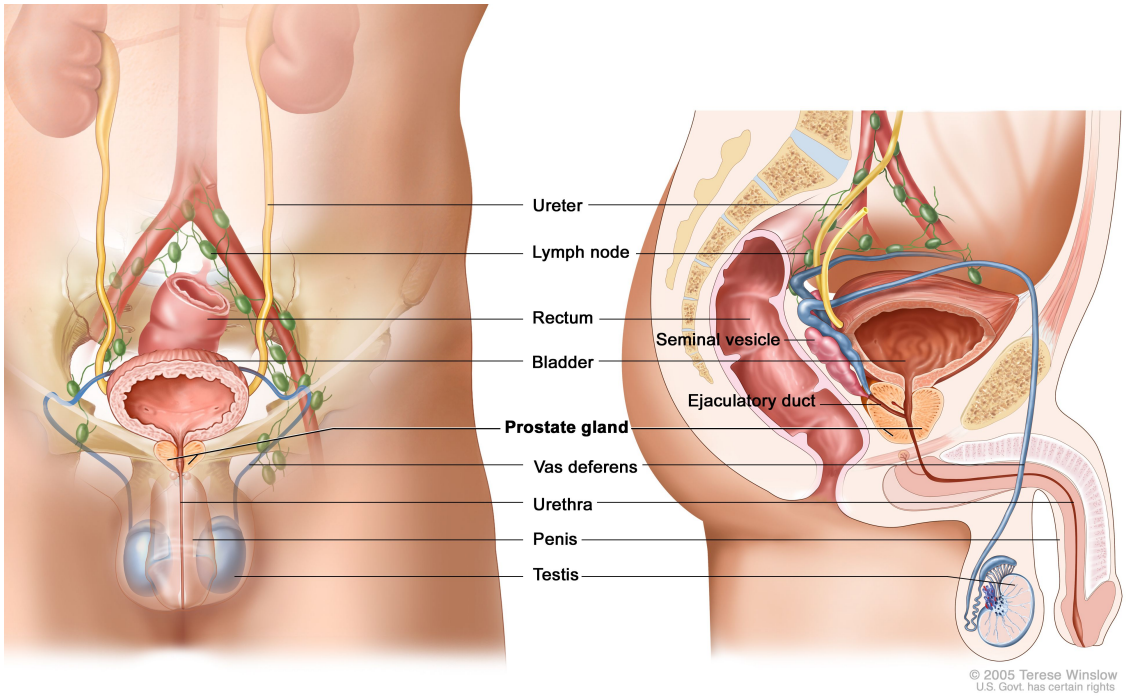

Figure 2.1: Pelvic region anatomy (from [2])

2.2 External Radiotherapy

The invention of radiotherapy goes back almost to the discovery of the X-rays when Emil Herman Grubbe treated a patient with breast cancer at the end of the XIX^{th} century. From then, it evolved quite rapidly with the discovery of the radium in 1898 by Marie and Pierre Curie and its physiological effects three years later by Marie Curie and Henry Becquerel. The low energy of the first X-rays was not appropriate for deeply located cancers, so the radiotherapy was mostly dedicated to skin cancer, but over the years, the techniques have improved, more powerful X-ray tubes have been developed, new radioactive elements have been discovered, which has extended the use of radiotherapy to almost all types of cancers.

The poor understanding of the biological effects of radiation combined with the lack of precision in the treatment delivery leaded to very small beneficial results compared to the side effects caused by the irradiation of healthy tissues for the patient, not to mention the exposure of the medical staff. Improvements needed to be done in the area of dose optimisation and toxicity reduction, and as early as the 1920s,

physicians started to understand that delivering the treatment dose in several fractions provides better results in term of cancer control and fewer side effects than in singular session. In fact, the body cells have natural mechanisms that can repair the damages done to the DNA by the radiations, especially when the lesions are small. But due to the loss of the replication checkpoints in the tumor cells, these mechanisms become far less efficient in the disease tissues than in the healthy ones. That's why leaving time between sessions of radiotherapy causes a reduction of the side effects for a given dose to the tumor. Then, in 1928, the International Commission on Radiological Protection (ICRP) was created to define the standards for radiation protection. In 1932, ionization chambers started to be used in order to accurately measure the doses delivered to the patients [3].

Many other improvements and techniques have been tried or implemented over the years, like the cobalt therapy in the 50s later abandoned in favor of more reliable and safer Linear accelerators (Linac), or the development of radiotherapy based on other particles, like electrons, protons and more recently carbon ions. But the biggest breakthrough in recent decades was the democratization of Information Technology (IT) in the hospital environment. The access to computers has caused a revolution in radiotherapy practices. The possibility to realise a complete 3D scan of each patient and the help of computers for simulations allow the physicists to create much more precise and complex treatment plans. In parallel, some hardware innovations have been made to precisely shape the radiation beam. First with the help of lead and Cerrobend (alloy of bismuth, lead, tin and cadmium) blocks, later with mechanical lead claws, and now using MultiLeaf Collimators (MLC). The MLC is composed of several "leaves" of high absorption material (usually tungsten) that can move independently and continuously during the treatment to shape the beams and therefore realize a very precise dose conformation on the tumor.

This leads to the techniques that we still use today, like the Intensity Modulated RadioTherapy (IMRT) which consists in changing the shape and intensity of each beam thanks to the use of a MLC. This technology is also called Dynamic MultiLeaf Collimator (DMLC) when the gantry is fixed during the irradiation, as opposed to the Volumetric Modulated Arc Radiotherapy (VMAT) which uses, in addition to the MLC, a continuous rotation of the gantry in order to spread the dose on the healthy tissues.

Some even more advanced techniques are currently used, like the Image Guided RadioTherapy (IGRT), which uses a Cone Beam Computed Tomography (CBCT)

before each radiotherapy session in order to check the tumor position once the patient is in place for treatment, and adjust the position of the table just before the delivery. The CBCT is a fast Computed Tomography (CT) technique that allows to take anatomically precise images in only one revolution around the patient, thanks to a cone shaped beam and a large plan detector. It is therefore much faster than conventional pencil beam CT, but at the cost of a lower precision in the measured densities, especially on the edges of the irradiation field.

Recently, online adaptive solutions have been released commercially. This technology is an improvement of the previous IGRT that can be implemented for DMLC and VMAT treatments. Its purpose is to overcome one of the weaknesses of the previous treatment modalities, that is the fact that the entire treatment plan is created based on a CT image taken at a certain time, with a given anatomy and position. The configuration is then assumed to be fixed for the whole treatment, which is an approximation that is not necessarily valid. In adaptive radiotherapy, the treatment system will therefore use a CBCT image taken before the session like in IGRT, but it will use it, not only to check the tumor position, but also, in combination to the original Computed Tomography simulation (CT-sim), to create a new treatment plan adapted to the current anatomy of the patient. This adaptation allows to ensure the dose coverage of the target, while optimizing the preservation of healthy tissues for the specific anatomy and position of the patient at the moment considered.

2.3 ETHOS treatment system

The ETHOS is a radiotherapy system produced by the company Varian Medical Systems. It is able to deliver adaptive radiotherapy treatments using CBCT imaging and Artificial Intelligence (AI).

What we call ETHOS is actually a combination of several components both hardware and software. The hardware part includes a Flattening Filter-Free (FFF) mono energetic linac of 6MV that produces the treatment beam and a 140kV linac-mounted Cone Beam CT imaging, both enclosed in a $2.6m$ diameter bore. As the ETHOS is delivering IMRT treatments, the gantry is equipped with a dual-layer MLC composed of two series of parallel tungsten leaves, one above the other with 29 and 28 pairs of leaves for the proximal and the distal series, respectively, for a total of 114 leaves. The leaves are $1cm$ wide and the two series are offset by $0.5cm$ from each

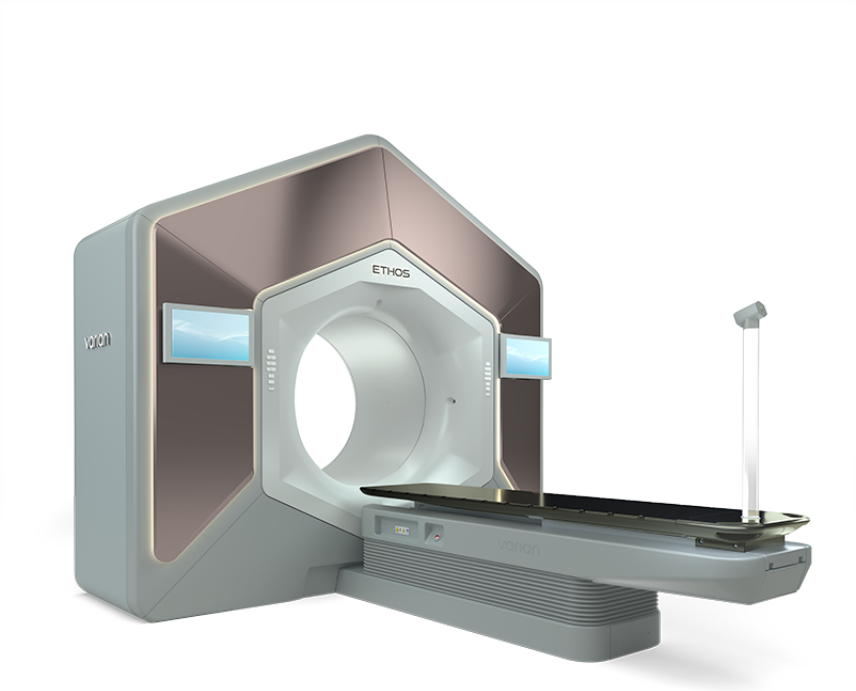

Figure 2.2: ETHOS treatment system. Image courtesy of Varian Medical Systems, Inc. All rights reserved.

other. This offset results in a $0.5cm$ wide area at the edge of the treatment field where the attenuation is weaker, which will slightly affect the penumbra of the beam [4]. The flattening filter was usually used to provide an approximately flat field, in order to provide the most uniform and homogeneous dose to the target. It is however no longer mandatory, as the MLC used in IMRT allows to reproduce any kind of photon fluence map, and therefore deliver homogeneous dose distributions.

To complete the hardware section, a treatment couch is provided with the system. This couch is made of carbon fiber in order to be sufficiently solid to support heavy patients while avoiding the imaging artefacts that a metal couch would cause. The lateral and longitudinal position is ensured by a set of electromagnets, which allows more precise positioning than mechanical adjustments. The height of the table is

set by a traditional mechanical system, as the electromagnets cannot carry the mass of a person while ensuring the precision required for patient positioning. Finally, a range of cameras, micros and speakers are provided to keep a connection between the patient and the control room [4].

The software part is also composed of several applications and algorithms to compute the dose, register the images, save and view the logs, etc. that are essential in clinical routine. In addition of that, an emulator is available online for research and training purposes. It perfectly reproduces the user interface and all the treatment steps of the actual ETHOS system. It is therefore possible to simulate the treatment of a real patient with different margins, treatment plans or workflows in order to compare the dose distributions, times of treatment, etc.

2.4 Workflow in adaptive radiotherapy

The clinical routine in adaptive radiotherapy is globally the same as in conventional radiotherapy (see figure 2.3).

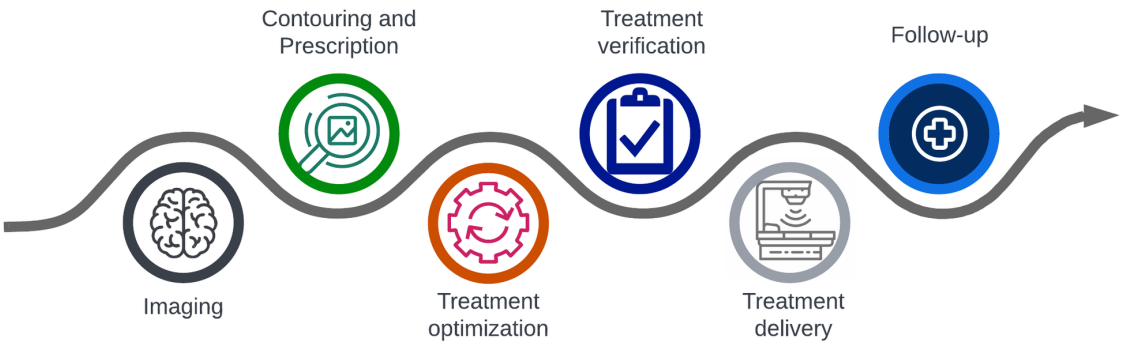

Figure 2.3: Scheme of the workflow in radiotherapy

The first step is the diagnosis. The radiation oncologist analyzes the patient records and all the imaging exams in order to identify accurately the pathology (stage the cancer, determine the eventual extension, etc.), and determines what will be the best treatment for the patient. Then, the latter gets an appointment with

his/her doctor, and they choose, together, which treatment will be done.

If a treatment with radiotherapy is chosen, they will schedule an appointment for the simulation step. It consists in performing a Computed Tomography (CT) scan, eventually in addition to Magnetic Resonance Imaging (MRI) for certain types of tumor. This scan will serve as a reference for all the treatment sessions, so it is essential that the images are of good quality, and that the patient is in a comfortable and reproducible position, as it would be kept identical during the whole treatment. In order to ensure that the position will be reproducible, the medical staff will make and/or use immobilization devices (like a mesh mask to immobilize the head, for example) that perfectly fit the patient's anatomy in the predetermined position so as to reuse them on the treatment table to reproduce the same position. Tattoos are made on the patient's skin using in-room lasers cross-hair. Before each treatment session, the patient will be aligned using tattoos and machine's in-room lasers, used to create a common reference coordinate system between the simulation and the treatment rooms.

Once the simulation is done, the physician delineates the tumor(s) on the CT scan images as well as all the Organs At Risk (OAR) in the target's surrounding region and makes dose prescriptions for the tumor. The volume of the tumor(s) delineated by the physician is called the Gross Tumor Volume (GTV), that is the visible part of the tumor. The Clinical Target Volume (CTV), the volume where there may be some tumor cells even if they are not visible on the images, is then automatically added to the GTV and modified by the physician based on his knowledge of the anatomy and of the properties of the specific type of the tumor being treated. Then, based on the prescription of the radiation oncologist and some dose constraints for the organs at risk, the radiophysicist or the dosimetrist realises the treatment plan with the help of a Treatment Planning System (TPS). This is a software that, given some constraints and the image from the CT-sim of the patient, will compute and optimize the dose distribution in order to meet the oncologist's prescription while preserving the healthy tissues. It also takes into account the technical parameters of the machine (configuration of the gantry, energy spectrum of the photons, etc.) to make a dose distribution deliverable by the system. In the specific case of the ETHOS system, the radiophysicist can choose between several fixed beam configurations : 3 arcs VMAT, 9 beams or 12 beams DMLC plans.

Once the treatment plan is satisfying, some patient-specific Quality Assurance (pQA) is performed before the treatment starts and consists in verifying the agree-

ment between the calculated and measured dose distributions. For example, a pQA that is made before each treatment start is the delivery of the treatment on a water-equivalent phantom inside of which is placed a 2D array of ionization chambers that measure the dose distribution. This dose distribution is then compared to the simulation using a gamma index[1]. In the CUSL, this step is realised using the Octavius 4D combined with the 2D-array Octavius 1500, both from PTW (PTW-Freidburg, Germany). Then, the patient is settled into place using the immobilization devices that were used during the CT-sim and the reference skin marks aligned with the in-room lasers system.

If the Quality Assurance (QA) is satisfactory, we can start to actually treat the patient. This will be done in several sessions, depending on the characteristics of the pathology. If the tumor is only present in the prostate and seminal vesicles, the treatment will usually have 20 fractions. If there is an invasion of the lymph nodes, there will more likely be 28 fractions. At last, for the irradiation of the prostate bed after a prostate ablation, a 26 fractions' treatment will be preferred, but this last kind of fractionnation was not considered in this work. The sessions are realised at a rate of one per day, five days a week for 4 to 6 weeks.

So far, the workflow in adaptive radiotherapy is just the same as in conventional IGRT. The differences come from the next step. In conventional IGRT and in adaptive radiotherapy, once the patient is correctly installed on the treatment couch, a CBCT of the pelvic region is made. Then, in conventional IGRT, the CBCT and the reference CT images are matched in order to adjust the position of the table. However, in adaptive radiotherapy, the CBCT image is used to perform a deformable registration of the CT-sim image to the acquired CBCT image. This process, realised by a CT-CBCT fusion algorithm, allows to match the Hounsfield Units (HU) (the measure of the radiodensities of the tissues, relative to water) of every pixel of the reference image with the anatomy of the patient, given by the CBCT. This new image is called a synthetic CT and will then be used by the treatment system to

[1]The gamma index is a metric used to compare two dose distributions. It is defined as :

$$\gamma(r_m) = min\left\{\sqrt{\frac{r^2(r_m, r_c)}{\Delta d_M^2} + \frac{\delta^2(r_m, r_c)}{\Delta D_M^2}}\right\} \forall\{r_c\} \tag{2.1}$$

with r_m the point of evaluation, r_c every other points of measurement, $r(r_m, r_c)$ the distance between r_m and r_c, $\delta(r_m, r_c)$ the dose difference between r_m and r_c, Δd_M a distance to agreement criterion (usually 2mm) and ΔD_M a dose difference criterion (usually 3%) [5]. This gamma index must be below 1 for 95% of the measurement points for the test to be passed.

create and optimize a new treatment plan adapted to the current anatomy of the patient. In order to be able to compute a new treatment plan, the system will first identify and create volumes, thanks to an AI, for some of the organs present on the image. For the prostate cases, it will identify the bladder, rectum, seminal vesicles, bowel (composed of the small bowel, the colon and the sigmoïd colon) and prostate. These volumes, called influencers, are then checked by the physician and modified if needed. The position of each influencer is then compared to its position in the CT-sim, and based on the displacements and deformations, a second structure-based fusion algorithm makes a prediction on the new position and shape of the CTV. This new volume is again checked and possibly modified by the physician, and once everything is correct, the adapted treatment plan is generated. Before delivering the treatment, this new plan needs to be verified. Indeed, the initial plan has been delivered to a detector in order to check if everything was all right, but it is impossible to do the same for the adapted plan, as it would imply to remove the patient from the treatment couch, and that would ruin all the previous work. The new treatment plan is therefore only virtually checked by using Mobius3D, a secondary plan calculation software provided by Varian, that uses a Collapse-Cone Convolution (CCC) algorithm. A global gamma index check with a 3%, 2mm criteria is then realised on the whole patient's dose distribution to compare the results from Mobius3D and the computation from the ETHOS, which uses Acuros, an algorithm based on solving the Boltzmann transport equations for photons and electrons. This comparison between two different algorithms would highlight an eventual beam modeling error in one of the two algorithms. Mobius3D will also recompute the dose distribution after the treatment using the log files saved by the system in order to identify any deliverability (hence mechanical) error.

The reason why we do not simply use the CBCT image to create the new treatment plan is because it cannot give sufficiently precise HU (or radiodensities) measures. Indeed, in order to give a fast image of a relatively large portion of the body, the CBCT uses a fan beam without an anti-scattering grid, which leads to much more noise in the final image compared to the pencil beam technology of the CT-sim, and therefore a deterioration of the measurement accuracy, especially in the edges of the field of view. The synthetic CT is then the combination of the accurate HU from the CT over the precise anatomy of the CBCT.

In parallel, the system simulates the dose distribution for the original treatment plan for the synthetic CT, in order to be able to oppose it to the adapted plan so that the physician can still choose the original plan in case issues occur during the

adaptation.

Finally, once the physician has chosen between the adapted and the original plans, a final CBCT is realised and matched with the previous one, to check for intrafraction changes during adaptation workflow. The position of the patient is then eventually adjusted, like in traditional IGRT workflow, before the irradiation. As the workflow in adaptive radiotherapy is much longer than in conventional radiotherapy, some displacements and changes in the patient's anatomy are more likely to happen. If the changes between the first and the second CBCT are too large, the workflow can be restarted based on this second image, or the patient may be removed from the table to restart the preparation steps. After that, the workflow is again the same as for conventional radiotherapy, with the saving of the fraction for QA and the release of the patient.

After the treatment, a follow-up is carried out by the physician to watch for specific signs or symptoms of recurrence, and, if necessary, take care of the long-term side effects of the treatments. The usual follow up tests are blood test for PSA and testosterone levels, and if any anomaly is detected, MRI or CT imaging are advised.

Chapter 3

Margins in radiotherapy

There are two types of margins in radiotherapy. The first one is called the CTV margin (see figure 3.1). Its goal is to take into account the microscopic and macroscopic extensions of the tumor into apparently healthy tissues, or to define the areas to treat when the tumor is not visible in the CT scan (e.g. for prostate cancer, one cannot see the tumor, so the CTV is defined as all of the prostate volume). This margin is purely clinical and is defined based on existing studies that used biopsies to determine the usual extensions of the tumors or by clinical experience.

The second type of margin is called planning target volume (PTV) margin (see figure 3.2). It is added to the CTV to ensure that it is properly covered by the irradiation dose despite all the uncertainties that could occur during any step of the treatment. In practice, it has to take into account the delineation uncertainty made by the physician, the setup errors (that includes the imprecision in the dose delivery of the treatment machine, the small changes in the patient's position between the fractions, the limited resolution of the imaging techniques, etc.), the changes in the anatomy of the patient from one session to the other (organ filling, ...) and the general intrafraction motion.

Ensuring that all patients get 100% of the dose on 100% of the tumor would require the irradiation of a very important volume, as the probability of a very large displacement of the tumor or that all uncertainties are adding up in the same direction may be small but never zero. It is therefore essential to find a compromise between tumor coverage and healthy tissue preservation.

This margin is defined in cooperation by the radiophysicists and the physicians, often based on a statistical study of the variations associated with all the different parameters.

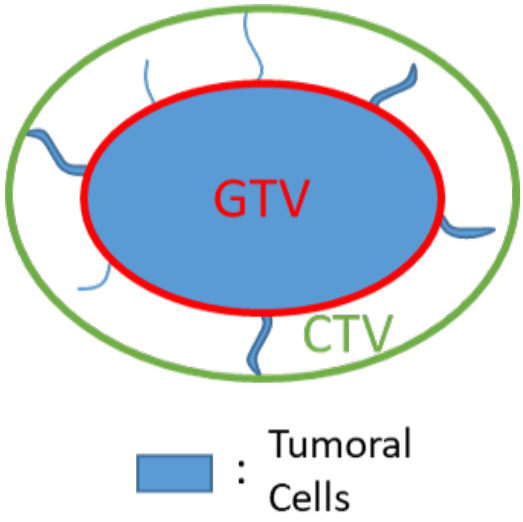

Figure 3.1: Representation of a tumor and its macroscopic and microscopic extensions, as well as a CTV that would properly cover all the tumoral cells.

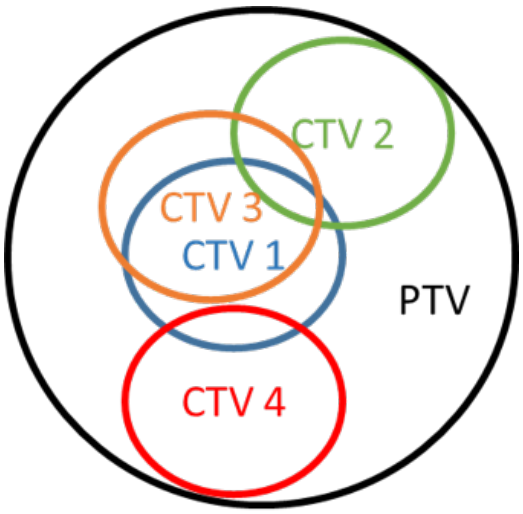

Figure 3.2: Representation of the CTV position changes through one radiotherapy treatment, as well as a PTV that would provide a 100% dose coverage of the CTV.

3.1 Van Herk margin recipes

In the late 1990s, Marcel Van Herk, a Dutch radiophysicist, realised that even if many studies had quantified the standard deviations of the vast majority of the possible errors that occur in radiotherapy, the radiophysicists still had some trouble using this mass of data and turn it into a usable margin. He therefore developed some simple recipes to compute the PTV margin that are comprehensive and can easily be transposed to clinical practice.

The basis of his reasoning lies in the assumption that there are two types of errors in radiotherapy that need to be treated independently. First, there are the systematic errors, which will be constant over the whole radiotherapy treatment for

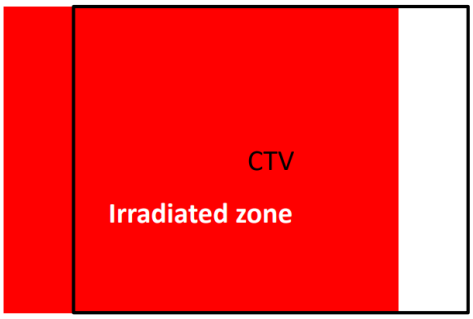

Figure 3.3: Effect of a systematic Left-Right error on the cumulative dose distribution (from [5]).

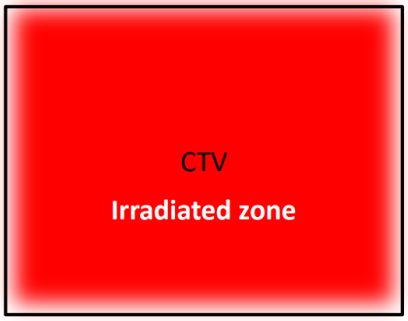

Figure 3.4: Effect of an isotropic random error on the cumulative dose distribution. Note the blurring on the edges of the irradiated field (from [5]).

one patient, but are stochastic in a population of patients. Within this category are usually found the delineation uncertainty and some of the setup errors, like the positioning uncertainties during the simulation, or a possible constant offset in the treatment table or beam positions. The standard deviations associated with these errors are usually denoted Σ. Then, there are random errors, that will change from one session to the other for a single patient or even during a single fraction. In this category, we find the daily variations in the patient's anatomy, the errors of positioning in the treatment machine, or the movements of the patient during treatment. The standard deviations associated with these errors are usually denoted σ.

The first type of errors will result in a shift of the cumulative dose distribution, which could lead to a complete miss of some part of the area to be irradiated (see figure 3.3). The second one will blur the dose distribution, resulting on a possible underdosage near the boundaries of the CTV (see figure 3.4).

3.1.1 Preliminary notes

The following development is a summary of the work of Marcel Van Herk et al., from an article published in the International Journal of Radiation Oncology, Biology, Physics in 2000, entitled: "The probability of correct target dosage: dose-population histograms for deriving treatment margins in radiotherapy" [6].

Before determining the various contributions of the systematic and random errors, some assumptions have to be made. The first one is that all sources of errors are random and not correlated and that we are in the central limit theorem conditions. This implies that the sum of the contributions of the errors follows a normal distribution, whatever are the real distributions of the individual errors. The mean of this new distribution is the sum of the means of all the individual distributions, and the standard deviation is given by :

$$\sigma^2 = \sum_i \sigma_i^2$$

with σ_i the standard deviation of each individual distribution.

The second assumption is that the medium is homogeneous, the CTV can be approximated by a sphere and there is no preferred area, this means that all parts of the CTV have the same importance and therefore must be covered the same way. The surrounding organs at risk are not considered and the dose distribution is idealized with a perfectly gaussian penumbra.

Finally, the fractionation effect is ignored. It means that we consider the treatment being split in an infinite amount of fractions. This simplification allows to consider the random and systematic errors independently.

3.1.2 Computation of the dose on a point CTV

The origin of the coordinate system used in the following development is the time-averaged position of the center of the CTV for the whole treatment (typically several weeks), and the reference time (T=0) is time at the CT-sim.

Let us first define the position of the CTV delineated on the scanner, noted $\mathbf{x_{deli}}$. Due to potential errors in delineation, patient position, organ movements, etc. the position delineated on the scanner is not $\mathbf{0}$, since the origin of the coordinate system is defined as the position of the CTV averaged on the whole treatment, but :

$$\mathbf{x_{deli}} = \mathbf{M}(0) + \mathbf{s}_0 + \mathbf{d} \tag{3.1}$$

with $\mathbf{M}(0)$ the CTV motion taken at the time of the scanner, $\mathbf{s}_0$ the setup error at the scanner and $\mathbf{d}$ the delineation uncertainty. All errors in equation 3.1 are system-

atic.

The real position $\mathbf{x}_n$ of the CTV for a given fraction n is similarly given by :

$$\mathbf{x}_n = \mathbf{M}(t_n) + \mathbf{s}_n \tag{3.2}$$

with $\mathbf{M}(t_n)$ the motion of the CTV taken at t_n, the time at the fraction n, and $\mathbf{s}_n$ the setup error at fraction n. All errors in equation 3.2 are random.

If $D(\mathbf{x})$ is the planned dose distribution at the point x and F is the number of fractions, the cumulative dose to the point CTV is given by :

$$D_{cum} = \sum_{n=1,\ldots,F} D(\mathbf{x}_n - \mathbf{x_{deli}})/F \tag{3.3}$$

By assuming a very high number of fractions, the sum over the fractions can be changed to an integral :

$$D_{cum} = \int P(\mathbf{y}) D(\mathbf{y} - \mathbf{x_{deli}}) d\mathbf{y} \tag{3.4}$$

with P($\mathbf{y}$) the probability density function of the position of the CTV and the integral covering the whole space.

By considering a symmetrical probability density, one can re-express the cumulative dose as the convolution of the probability density and the dose distribution :

$$D_{cum} = (P(\mathbf{y}) \otimes D(\mathbf{y}))_{\mathbf{y}=-\mathbf{x_{deli}}} \tag{3.5}$$

For the following, $G(\mathbf{x}; \sigma^2)$ is the gaussian distribution with a mean of 0 and a variance σ^2. By the central limit theorem, we consider the total random error as a gaussian with zero means. The probability density of the position of the CTV is then :

$$P(\mathbf{y}) = G(\mathbf{y}; \sigma^2_{\mathbf{rand}}) \tag{3.6}$$

with $\sigma^2_{\mathbf{rand}}$ the variance of the random error, define as the sum of the variances of every contribution.

In order to evaluate equation 3.5, we need to define the shape of the dose distribution D. By definition of the penumbra, the dose distribution can be expressed as the convolution of a gaussian and a radial step function S defined as :

$$S(\mathbf{x}, w) = \begin{cases} 1 & \text{for } |x| \leq w \\ 0 & \text{for } |x| > w \end{cases} \tag{3.7}$$

The dose distribution is then :

$$D(\mathbf{y}) = D_{nominal}(G(\mathbf{y}; \sigma^2_{\mathbf{p}}) \otimes S(\mathbf{y}, w)) \tag{3.8}$$

with $D_{nominal}$ the nominal total dose and $\sigma^2_{\mathbf{p}}$ the variance of the penumbra.

The dose blurred by random errors is then :

$$D_{blurred}(\mathbf{y}) = D_{nominal}(G(\mathbf{y}; \sigma^2_{\mathbf{p}} + \sigma^2_{\mathbf{rand}}) \otimes S(\mathbf{y}, w)) \tag{3.9}$$

and the cumulative dose to the CTV is :

$$D_{cum} = D_{blurred}(-\mathbf{x_{deli}}) \tag{3.10}$$

This last equation can be generalised to an extended CTV by adding a parameter $\mathbf{y}$ that describes the position of a point in the CTV relative to a reference point, like the center of mass. In that case, $\mathbf{x_{deli}}$ is the delineated position of the reference point, and $\mathbf{x_n}$ is the position of the reference point. Equation 3.10 becomes :

$$D_{cum}(\mathbf{y}) = D_{blurred}(\mathbf{y} - \mathbf{x_{deli}}) \tag{3.11}$$

3.1.3 Probability of delivering a certain dose to a point CTV

The probability that the cumulative dose to the CTV exceeds a certain value $D_{threshold}$ is given by :

$$P(D_{cum} > D_{threshold}) = \int_C Q(\mathbf{z}) d\mathbf{z} \tag{3.12}$$

with Q the probability density of $\mathbf{x_{deli}}$ and C the collection of $\mathbf{x_{deli}}$ for which $D_{cum} > D_{threshold}$, thus defined as :

$$C : \{\mathbf{x_{deli}} | D_{blurred}(-\mathbf{x_{deli}}) > D_{threshold}\} \tag{3.13}$$

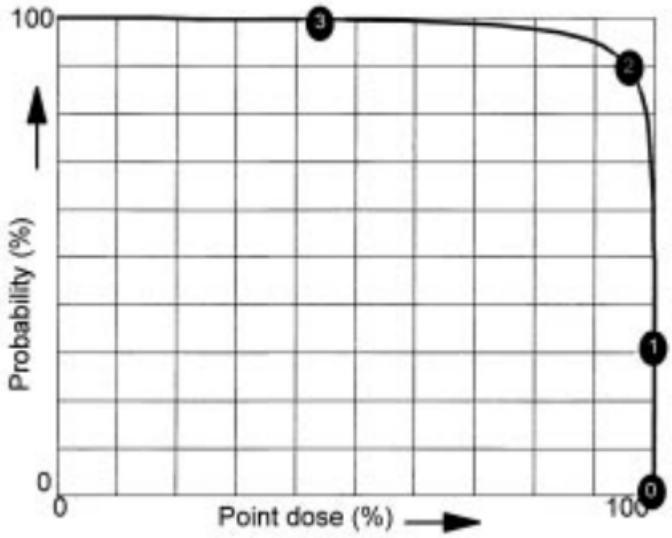

Figure 3.5: Example of a dose-population histogram for a point CTV and arbitrary margin and errors (from [6]).

By plotting equation 3.12 as a function of $D_{threshold}$, we obtain a dose-population histogram (see figure 3.5), representing the probability of the cumulative dose over a population of patient.

Due to the previous assumptions that the errors are not correlated and that their sum follows a normal distribution, the probability density Q may be written as :

$$Q(\mathbf{z}) = G(\mathbf{z}; \Sigma^2_{\mathbf{sys}}) \tag{3.14}$$

where $\Sigma^2_{\mathbf{sys}}$ is the variance of the systematic errors, defined as the sum of the variances of all contributions.

Again, this expression can be generalized for an extended CTV by adding a *dose* parameter :

$$P(dose > D_{threshold}) = \int_C Q(\mathbf{z}) d\mathbf{z} \tag{3.15}$$

3.1.4 Computation of the required margin

In equation 3.15, the new *dose* parameter has not yet been clearly defined, because it is dependent on the objectives of the margin. Indeed, determining a margin required to compromise between dose coverage and preservation of healthy tissues, and these compromises will be expressed as dose or tumor control probability objectives. These may be very different and some examples are given in table 3.1. The objective that Van Herk used for his works, and that is now used to compute the majority of the margins in radiotherapy, is the following : "for 90% of the patient population, the minimum dose to the CTV must be 95% of the nominal dose (i.e., the dose at the specification point) or higher." [6].

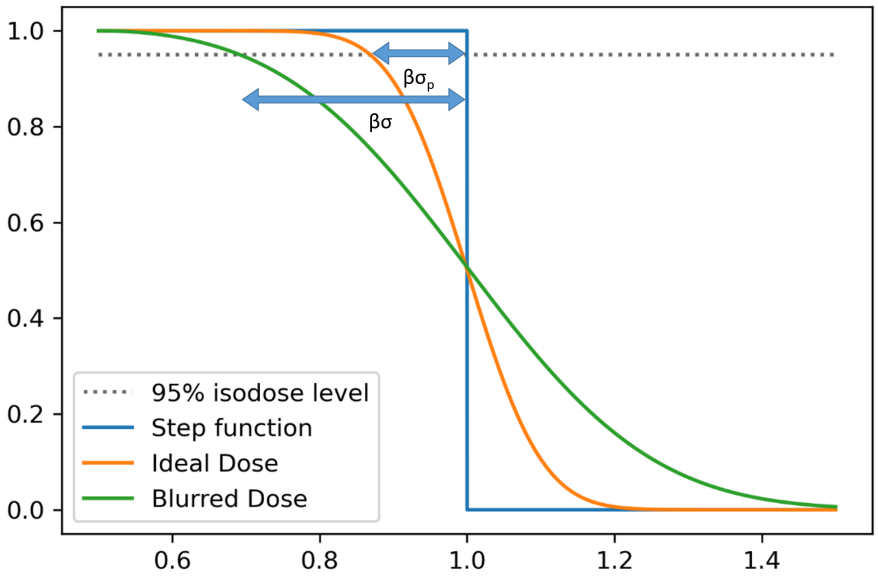

Figure 3.6: Illustration of the edge of idealised dose distributions with only the penumbra taken into account in orange, and with all random errors in green. Both axis use arbitrary units.

For the treatment margin, one must find a collection C in which 90% of the preparation errors fall using equation 3.15. This is done by using the assumption that the preparation errors follow a normal distribution with a standard deviation

$\Sigma_{\mathbf{sys}}$. In 3 dimensions, the normal distribution is :

$$G(x, \Sigma_{sys}^2) \cdot G(y, \Sigma_{sys}^2) \cdot G(z, \Sigma_{sys}^2) \tag{3.16}$$

and the probability for the norm of the vector $\mathbf{r} = (x, y, z)$ to be smaller than a certain value w is given by :

$$\int_0^w \frac{r^2}{\sqrt{\frac{\pi}{2}} \cdot \Sigma_{sys}^3} \cdot \exp\left\{-\frac{r^2}{2\Sigma_{sys}^2}\right\} dr \tag{3.17}$$

By solving this integral and plotting the result as a function of w/Σ_{sys}, we obtain probability curves and a required margin of $2.5\Sigma_{sys}$ for the preparation errors.

To this preparation margin must be added the treatment execution margin. As we set as an objective to ensure 95% of the nominal dose to the CTV, the margin is basically the difference between the 95% isodose of the planned dose and the same isodose for the blurred dose distribution. By taking the 50% isodose as a reference (as this surface doesn't move with the blurring, see figure 3.6) we find that the difference between the two 95% isodoses is simply $\beta\sigma - \beta\sigma_p$ with β a parameter that is equal to 1.64 for the 95% isodose, σ the standard deviation of the total random error, penumbra included, and σ_p the standard deviation of the penumbra.

Finally, the total margin required for the objective that has been set is :

$$\mathbf{m_{PTV}} = 2.5\Sigma_{\mathbf{sys}} + 1.64(\sigma - \sigma_{\mathbf{p}}) \tag{3.18}$$

This margin recipe is the one that has been used in this entire work.

Other configurations exist in literature, depending on which errors are taken into account and which objectives are set. These objectives may be expressed as dose coverage or minimal dose to the CTV, like in Van Herk et al. work, or as Tumor Control Probability (TCP) loss, which is an evaluation of the probability for the treatment to fail to eradicate or control the tumor (see table 3.1).

Authors	Recipe	Description
Bel et al. [7]	0.7σ	Linear approximation for random errors only
Stroom et al. [8]	$2\Sigma + 0.7\sigma$	95% dose on 99% of CTV for realistic plans[1]
Van Herk et al. [9]	$\sqrt{2.7^2\Sigma^2 + 1.6^2\sigma^2} - 2.8mm$	Margin for 1% of TCP loss due to geometrical errors for prostate patients

Table 3.1: Margin recipes proposed by several authors. Σ is always the standard deviation of the total systematic error, and σ the standard deviation of the total random error [10].

3.2 Previous margin for prostate treatment

Until now, the margin used for the adaptive treatments of prostate cancers in the radiotherapy department of the CUSL was an isotropic margin of 7mm. This value comes from the margin previously computed by Van Herk et al. [6] for conventional IMRT, using data from Rasch et al. [11], Van Herk et al. [12] and Bel et al. [7] for the computation of the standard deviations of the errors, adapted for IGRT. They made the hypothesis that the IGRT is perfect, allowing them to neglect the setup and organ motion errors. The only contributions considered were then the delineation and intrafraction motion that lead respectively to a systematic margin of $6.3mm$ and a random margin of $0.7mm$.

Even if these simplifications may seem exaggerated, as the IGRT does not correct all the errors, this margin has nevertheless proven itself, as shown by the work of Gill et al. [13] or Gupta et al. [14] among others.

[1]Realistic plans means that instead of making a mathematical computation of the margin required based on the probability distributions of the errors, a range of fictional treatments are simulated in which realistic errors are made, and the PTV is defined as the minimum volume for which all or a given proportion of the simulated treatments are satisfying.

Chapter 4

Methods

The aim of this work is to compute the required PTV margin for the adaptive radiotherapy treatment of prostate cancer by identifying and computing all the different contributions.

I analyzed 10 prostate cancer patients treated between August 2021 and April 2022 with adaptive radiotherapy using the Varian ETHOS machine in the CUSL (Cliniques Universitaires Saint-Luc). Those 10 patients were treated with a total of 208 fractions (9 times 20 fractions and once 28). Among them, 11 fractions have been removed due to the lack of a second control CBCT image acquired just before irradiation, and 28 were ignored because of technical problems during the exportation from the ETHOS system, that made the structures set unavailable. This leaves 169 radiotherapy sessions to analyze.

All the scripts mentioned in this work have been written and ran using Spyder 5.1.5 and Python 3.9.7. When needed, I used the packages numpy 1.20.3, scipy 1.7.1, pydicom 2.2.2 and matplotlib 3.4.3. For the basic analysis of the results, I used Microsoft Excel 2019 and LibreOffice Calc 7.3.2.2.

4.1 Setup margin

The setup margin is the margin related to the capacity of the system to properly place the patient during both the simulation CT and each fraction as well as its mechanical capacity to aim at the target.

In adaptive radiotherapy, and in IGRT in general, the setup errors are particularly low, thanks to the position check of the patient before each session. The only

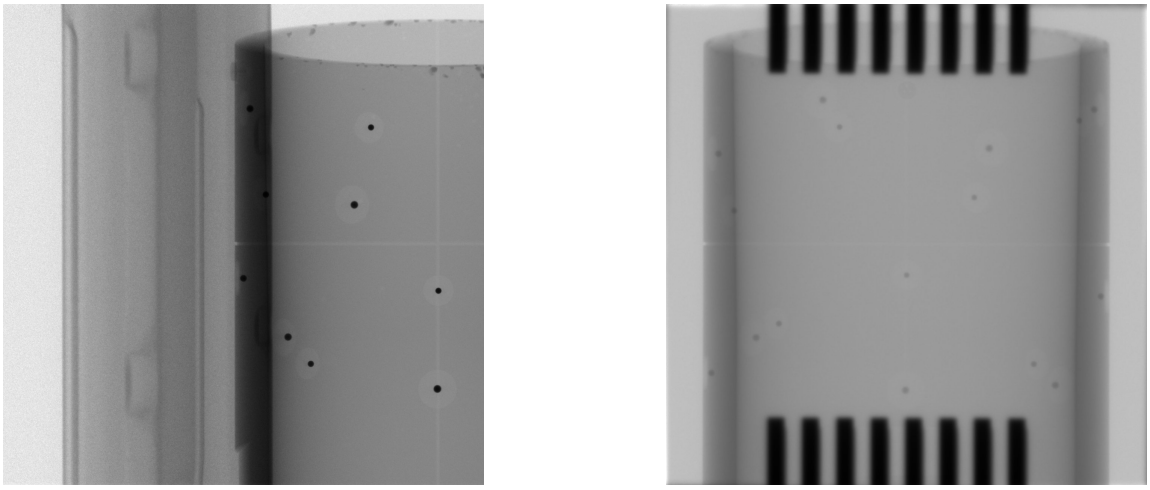

Figure 4.1: kV and MV images of the Drum phantom

significant error that remains is the difference between the treatment isocenter and the imaging isocenter, which is caused by imprecision in machine manufacturing and configuration. It will then obviously not change a lot between two different fractions or even two different patients, so it is expected to be mainly a systematic error.

The data required to determine this difference are already available, as the ETHOS automatically measures it every morning as part of the machine performance checks (MPC). In practice, the physicist fixes a Drum phantom, which is an empty cylinder with 16 radiopaque markers placed on its surface, at the isocenter of the treatment system. The latter will then deliver a fixed pattern of both kV and MV beams in order to evaluate the beam's and machine's mechanical parameters. It uses the markers as a static reference to determine the distance between the center of the imaging system and the center of the treatment system (see figures 4.1). To evaluate the setup error, we have extracted the records of the MPCs since the beginning of the treatment of the first patient, on the 19^{th} of August, 2021, until December 2^{nd}, 2021. That represents 88 measurements, the average of which can be calculated to find both systematic and random components of the error.

In the setup error, one could also consider the accuracy of the movement of the table, or of the gantry, but in the particular case of the ETHOS treatment system, these are at least one order of magnitude smaller than the other errors (typically 0.05mm). As they should be quadratically added, we choose to neglect their individual contributions.

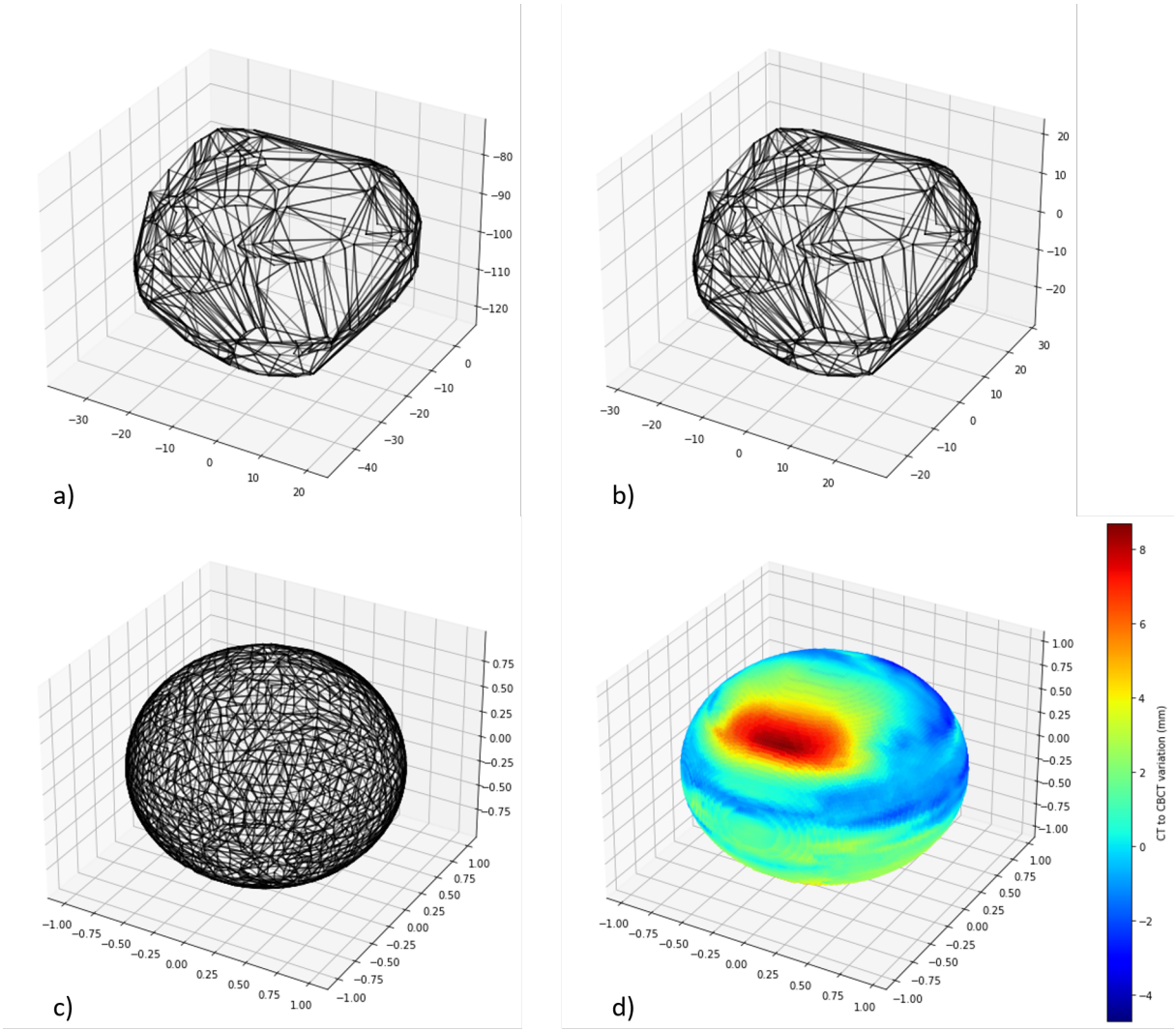

Figure 4.2: Main steps of the workflow to compute the delineation uncertainty.
a) The contour point coordinates of the prostate delineation are extracted from the simulation CT and the CBCT RTSTRUCT files.
b) The COM of both are computed, and the two structures are centered on them.
c) All the points are contracted and interpolated to a predefined grid over a unit sphere. The distances between each point and the center of mass are kept in separate matrices.
d) The difference of the distance matrices is mapped to the sphere and split into the six directions in space in order to compute the mean uncertainty for every one of them.

4.2 Delineation margin

The delineation margin is usually considered as fully systematic, because in conventional radiotherapy, the delineation is only made once, on the simulation CT-scan. In adaptive radiotherapy, the delineation is modified by the ETHOS algorithm, verified and eventually adapted by a physician before each fraction. It is therefore legitimate to split the error into a random and a systematic contribution. Moreover, in the radiotherapy department of the CUSL, even the physician in charge of the verification of the delineation will change from one fraction to the other, as they are not assigned to patients, but to all patients in given time slots, for time-optimization purposes. This particularity adds even more randomness in the delineation uncertainty.

To discriminate the random variation from the systematic one, I transferred, for each patient, the prostate contour delineated on the first CBCT of every session to the simulation CT using Eclipse treatment planning system 16.1 by Varian (Varian Medical System, USA). I then extracted the structure set containing all the prostate contours and wrote a Python script (see Appendix A) to evaluate the variation between all contours. The method used is based on the work of Remeijer et al. [15] to quantify the 3D variations of the delineated volume but for the Python implementation, which is completely new. Their method was chosen here because it is an effective way to quantify both the systematic and the random volume variations in all 6 directions of space for nearly spherical CTV volumes. Moreover, the outcomes are immediately computed in a form that is compatible with the Van Herk margin recipe.

This script first computes the Center Of Mass (COM) of each structure in order to express the coordinates of each point of the structure relative to its center. The next step is to compute the coordinates of each point projected onto the surface of unit sphere while keeping track of its original distance to the COM. This step is realised by switching to spherical coordinates, normalizing each position vector and returning to cartesian coordinates. Once we have a unit sphere of points with values attached, we interpolate the values for every structure onto the same meshgrid in order to define a common coordinate system to compare the distances to the COM. It then keeps only the edges of the data matrices in all directions, to isolate the actual contour of the volume, and computes the value differences between the corresponding points from the representation of the prostate in the CT geometry and its representation in the daily CBCTs. Finally, it segments the results into 6 areas corresponding to the 6 directions (right, left, anterior, posterior, cranial and caudal)

and compute the mean difference for each part. The 6 areas are defined as all the points situated between +45° and -45° in both directions, relative to the axis pointing in the considered direction. For each patient, the script returns the mean variation in every direction and the standard deviation between the different sessions. Given this information, we can find the systematic standard deviation Σ by computing the standard deviation of the means of the patients and the random standard deviation σ by computing the root mean square of the individual standard deviations.

In order to be able to extract actual values for the random and systematic contributions of the delineation uncertainty, some assumptions had to be made. The first one is that the movements of the prostate are only translations, and there are no rotations of any kind. The second one is that there are no variations of the shape of the prostate through the treatment, and the last one is that for every patient, the delineations done by the physicians on the CT-sim are correct. These assumptions allow to match all the contours in a common coordinate system and compare their shapes point by point.

4.3 Intrafraction motion

The intrafraction motion is, most of the time, considered as a fully random margin contribution, as it changes with a period smaller than the duration of one fraction, and then obviously smaller than the duration of the whole treatment. One can however imagine that the patients may have some systematic movements as they relax during the time they are lying down the same way for each session. We therefore decided to realise a full study of the intrafraction motion without assuming that there is only a random component.

As mentioned in section 2.4, there are two different CBCT taken during each treatment fraction. The first one is needed to optimize the adaptive treatment and the second one to check if the patient has not moved too much during the optimization process. These two images are taken within a time interval of 10 to 30 minutes, approximately, and we made the assumption that the movement we can see between the two images is a good estimator of the movement during treatment delivery.

In order to measure the movement between the two CBCT, I realised a soft tissues' based rigid registration of the second CBCT to the first one so as to match

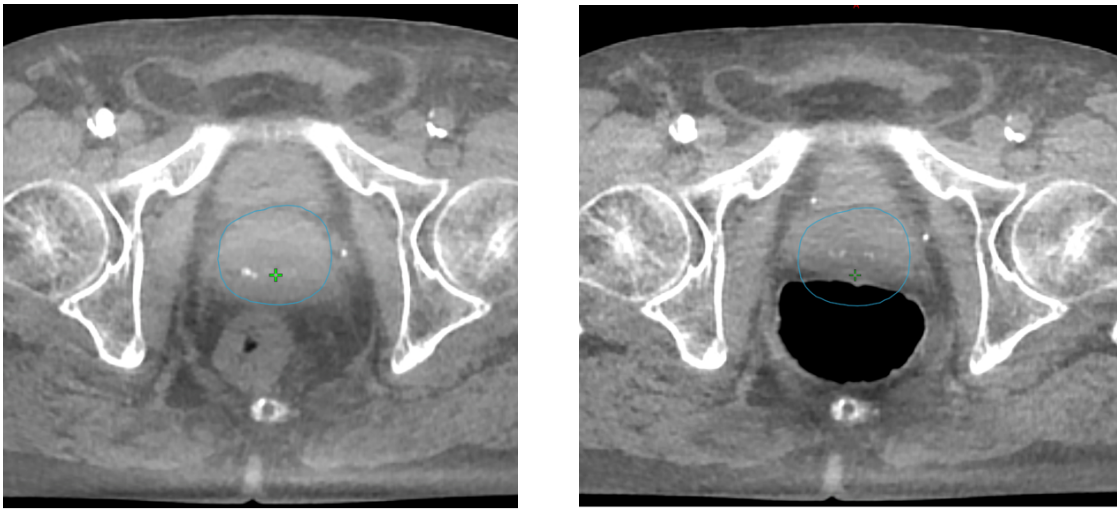

Figure 4.3: Comparison of the CTV position and shape in the two CBCT images of a single fraction of a patient. The variation from one image to the other is particularly high, due to a large rectum volume variation.

the prostates on both pictures. I have done that by using Eclipse treatment planning system 16.1 by Varian and helped myself with the automatic registration tool provided with it before making some manual adjustments to obtain the best visual match. I then saved the registration parameters to an Excel file.

The manual registration part may be one of the major sources of errors in this work. Therefore, in order to make an evaluation of them, I asked a physician to do the same work as I did for ten randomly selected sessions (one for each patient). The results were then compared to mine and a standard deviation of the variation was computed.

4.4 Penumbra

For conventional Linac, equipped with a flattening filter, the standard deviation associated to the penumbra is defined as the standard deviation of the gaussian function with which one needs to convolve a step function in order to obtain the measured dose profile. In this case, we consider the dose distribution in a water-

equivalent phantom at 10cm depth, placed at the isocenter of the treatment beam, for a field size of $10 \times 10cm^2$. We assumed that the dose distribution is well represented by the convolution of a truncated parabola and two gaussians with different standard deviations. We use here a truncated parabola instead of a step function because the ETHOS system uses a FFF beam. To find the parameters, I computed the convolution of the three functions (python code given in Appendix B) and I adapted the parameters of the truncated parabola to obtain the best visual match.

Chapter 5

Results

5.1 Setup Margin

The 88 measurements of the position of the imaging isocenter, relative to the treatment isocenter, give a mean deviation of 0.3mm and a standard deviation of 0.05mm. The later will be neglected for obvious reasons, and we will only keep a systematic contribution of 0.3mm in all directions.

5.2 Penumbra

The curve_fit function returns two standard deviations for the convolution gaussians of 2.78mm and 0.1mm. We can consider that the second gaussian is negligible compared to the first one, so we will keep a penumbra of 2.8mm. The penumbra difference between the two directions in the plane perpendicular to the beam being negligible, we will consider the penumbra as isotropic.

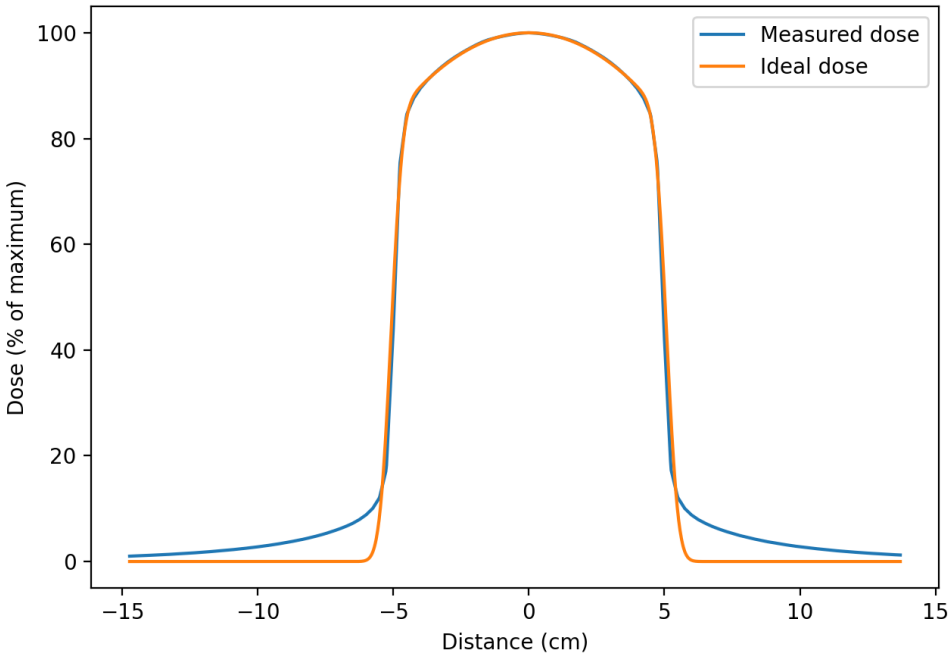

Figure 5.1: Dose profile at 10cm and analytical fit using parabola and gaussian functions

5.3 Intrafraction motion

The global mean intrafraction motion, the standard deviation of the mean motions of every patient and the root mean square of the standard deviations of each patient are given in table 5.1.

The mean motion and the standard deviation of every patient are represented in figure 5.2.

As a reminder, the standard deviation of the means will be a contribution of the systematic error, and the root mean square of the standard deviations will be the random contribution. The global mean is not used in the margin computation, and is given for information only.

In the following table, a positive value in the Left-Right (LR) direction corre-

sponds to a displacement to the left, a positive value in the Anterior-Posterior (AP) direction corresponds to a displacement to the anterior direction, and a positive value in the Cranial-Caudal (CC) direction corresponds to a displacement to the caudal direction.

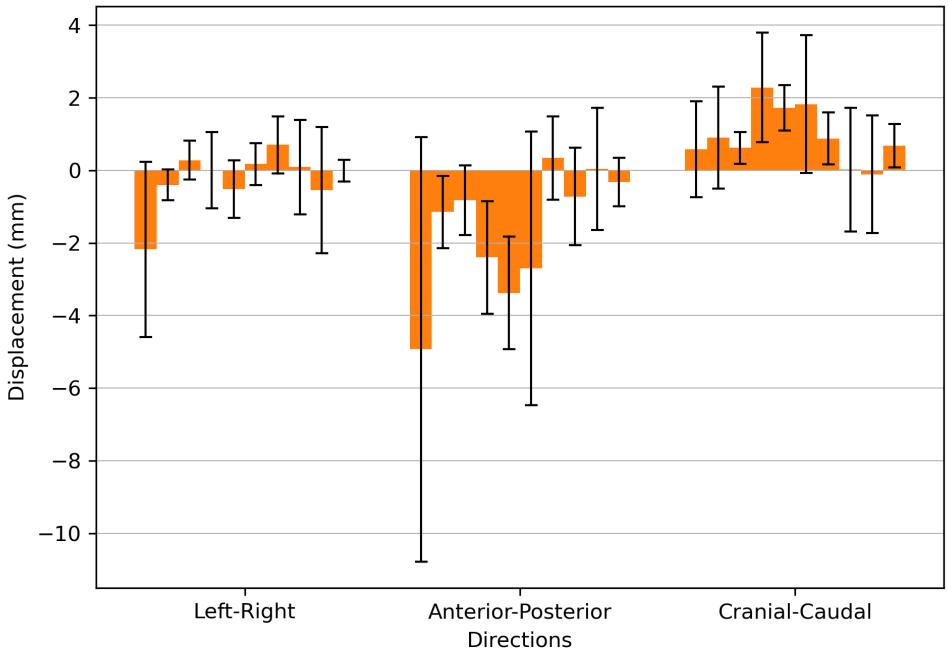

Figure 5.2: Mean and standard deviations of the intrafraction motion of every patient for the three directions.

Intrafraction motion (mm)			
	Left-Right	Anterior-Posterior	Cranial-Caudal
Global mean	-0.24	-1.67	0.99
Standard deviation	0.78	1.69	0.78
Root mean square	1.18	2.48	1.29

Table 5.1: Summary table of the intrafraction motion errors. The global mean is the mean movement of the entire population of patients, the standard deviation is the one of the mean motions of every individual patient, and the root mean square is the RMS of the intra-patient's standard deviations.

5.4 Delineation

The results for the delineation uncertainties are given in table 5.2 and represented in figure 5.3. Like for the intrafraction motion, the standard deviation of the means will be a contribution of the systematic error, and the root mean square of the standard deviations will be the random contribution. The global mean is not used in the margin computation, and is given for information only.

Delineation uncertainty (mm)						
	Left	Right	Anterior	Posterior	Cranial	Caudal
Global mean	0.07	-0.18	0.06	0.12	-0.03	-0.27
Standard deviation	1.03	0.96	1.03	0.74	1.80	1.06
Root mean square	1.35	1.31	1.47	1.12	1.67	1.41

Table 5.2: Summary table of the delineation uncertainty. The global mean is the mean error of the entire population of patients, the standard deviation is the one of the mean errors of every individual patient, and the root mean square is the RMS of the intra-patient's standard deviations.

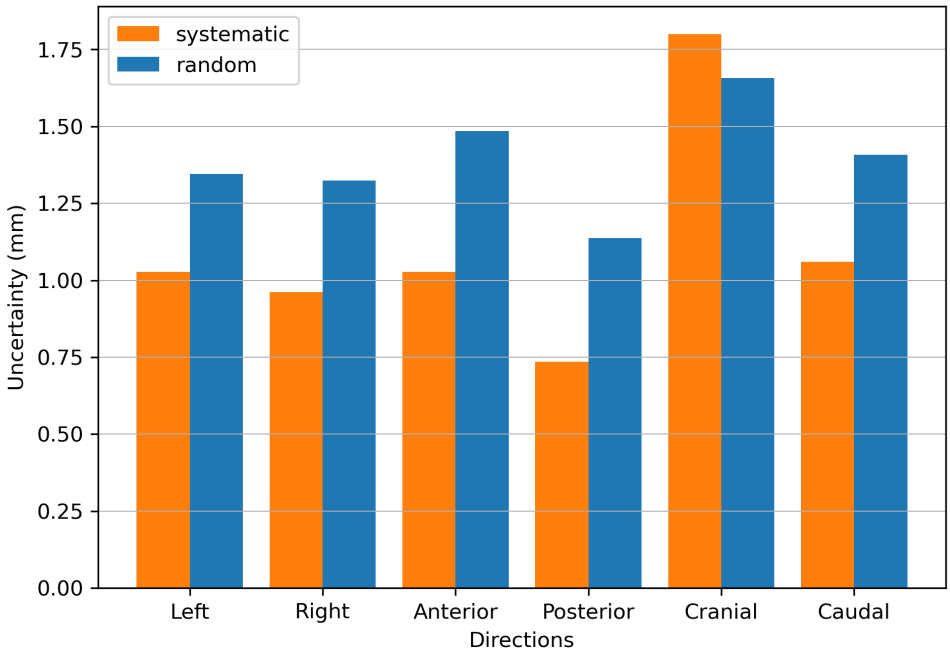

Figure 5.3: Random and systematic delineation uncertainties.

5.5 Total margin

Summary tables for systematic and random errors are given in table 5.3 and 5.4 respectively. The totals displayed are the quadratic sum of all the contributions, as they are standard deviations of independent random variables.

Systematic errors (mm)						
	Left	Right	Anterior	Posterior	Cranial	Caudal
Delineation	1	1	1	0.7	1.8	1.1
Setup	0.3	0.3	0.3	0.3	0.3	0.3
Intrafraction motion	0.8	0.8	1.7	1.7	0.8	0.8
Total	1.3	1.3	2	1.9	2	1.4

Table 5.3: Summary table of the systematic errors for every direction and every category.

Random errors (mm)						
	Left	Right	Anterior	Posterior	Cranial	Caudal
Delineation	1.3	1.3	1.5	1.1	1.7	1.4
Intrafraction motion	1.2	1.2	2.5	2.5	1.3	1.3
Penumbra	2.8	2.8	2.8	2.8	2.8	2.8
Total	3.3	3.3	4	3.9	3.5	3.4

Table 5.4: Summary table of the random errors for every direction and every category.

We can now compute the total margin using the exact Van Herk formula :

$$M_{PTV} = 2.5 \times \sqrt{\Sigma^2} + 1.64 \times \sqrt{\sigma^2 + \sigma_p^2} - 1.64 \times \sigma_p$$

with Σ the total systematic error, σ the total random error and σ_p the penumbra.

The results are given for every direction in table 5.5.

Total margin (mm)					
Left	Right	Anterior	Posterior	Cranial	Caudal
4.4	4.3	7.2	6.7	6.3	4.6

Table 5.5: Total margin in every direction

In the following, this margin will be called the final margin.

Chapter 6

Discussion

The numerous changes introduced in the radiotherapy workflow by the adoption of adaptive radiotherapy require to adapt all the steps of patient management. It includes the adaptation of PTV margins in order to take the utmost advantages of this new technique. Moreover, some aspects of the margin recipe depend on the type of machine used and others are bound to the particularities of each hospital (patient preparation protocols, used of MRI images acquired in treatment position, etc.), and should therefore be computed in every radiotherapy department for an optimal precision.

This is especially true for the intrafraction motion, since it is greatly influenced by the management of the patient and the treatment's protocol. It may change a lot according to the urination protocols established, the patient's medication to help emptying the rectum, etc. and depending on the time spent on the influencers and CTV checks, which are function of the performance of the ETHOS's AI, but also of the staff training.

The adaptive radiotherapy is also a treatment modality that allows to consider the delineation uncertainty to be partly random and not fully systematic. Since it was not the case with the traditional IGRT and DMLC, there is still a lack of literature on this topic. Moreover, quantifying the variability of the delineation usually requires substantial resources, such as a pool of physicians, delineating the same patient several times. This is needed to determine the inter-observer and intra-observer variations. These resources are already available in the CUSL, thanks to the particular workflow of adaptive radiotherapy, that implies the daily delineation of the target by a physician, who changes from one day to the other. The delineation uncertainty may slightly change from one medical center to another, depending on the staff training, of course, but also on the availability and quality of MRI or Flu-

oroDeoxyGlucose Positron Emission Tomography (FDG-PET) images to help the physicians in the delineation.

6.1 Setup

In the margin used so far, the setup error was considered to be negligible for IGRT treatments. This assumption can not be verified since there is a lag between the isocenter of the treatment beam and the imaging beam. So even considering that the precision of the IGRT is perfect, the system will never be able to replace the patient with a precision greater than this lag.

As explained in the Methods chapter, the parameter used to determine the setup error is the distance between the imaging isocenter and the treatment isocenter. The exact behaviour of the positions of the two isocenters is still unknown, which means that they may stay fixed one with respect to the other, but they may move with the rotation of the gantry. In the first case, the error should therefore be fully systematic, but in the second one, it will be random. To be sure not to underestimate the margin, the choice has been made to consider this error as fully systematic, by precaution principle. In either case, this error is very low, compared to the other contributions, therefore a wrong categorization would only have a minor impact.

6.2 Penumbra

As mentioned earlier, the penumbra of the beam is usually defined as the standard deviation of the gaussian by which a perfect square beam needs to be convoluted to obtain the measured dose distribution. But in the specific case of the ETHOS, which is not equipped with a flattening filter, the perfect dose profile is not a square function, but a truncated parabola. The same type of analysis can still be done to determine the penumbra, as it doesn't change the shape of the edges of the dose profile.

The resulting value of $2.8mm$ is in agreement with the value of 2.9mm obtained by E. Sterpin and D. Dechambre [16], which has been computed with the same system in the CUSL and is now the reference value for clinical routine. It is slightly smaller than the usual $3.2mm$ penumbra used in margin computation [6], but that difference can be explained by the use of a FFF beam, knowing that a filter always

increases the scattered radiation, and therefore the penumbra, and by the particular configuration of the MLC, which is composed of two staggered layers of leaves, preventing the leak of photons in the gaps between two successive leaves. The particular configuration of the MLC also contributes to the opposite effect, as the staggering of the leaves causes a $0.5cm$ strip at the edges of the irradiation field where the beam is only stopped by one layer of tungsten instead of two. This reduction of the penumbra for FFF beams and the smaller effect of the geometry of the MLC are in line with the 15% reduction of the penumbra measured by Pönisch et al. [17] on a different system, but with similar MLC and beam configurations.

The particular configuration of the MLC, with two staggered layers of leaves instead of one layer and two jaws, also allows to consider the penumbra as isotrope, since the beam is attenuated by the same leaves in every direction, and not by the leaves in one direction and the jaws in the other, which leads to an asymmetry in the penumbra.

6.3 Intrafraction motion

The intrafraction motion is the most important contribution to both the systematic and the random errors for nearly every direction. The usual IGRT margin was considering a $1mm$ isotropic fully random error for the intrafraction motion, which is far from the results obtained. Other studies using prostate tracking devices show smaller intrafraction motion errors than the ones obtained in this work (see table 6.1) for treatment times ranging from 2 to 10 minutes. This can be explained by the time interval between the two CBCT used to evaluate the errors, which ranges from 10 to more than 30 minutes. The probability that the patient has moved is therefore much more important. Indeed, if we compare our results with the ones obtained by Mayyas et al. [18] or Badakhshi et al. [19] with similar time intervals, the differences are much smaller. As the real irradiation time after the second CBCT is less than 5 minutes, and based on the information provided by the studies above, the assumption made that the movement between the CBCT is a good estimator of the intrafraction movement may be questionable.

Another point worth mentioning is that the global mean movements, which are not considered in the margin computation, are not negligible, especially in the AP and CC directions. This global movement, in the posterior and caudal directions,

	LR [Δ]	AP [Δ]	CC [Δ]
Systematic (mm)	0.5 [-0.3]	0.9 [-0.8]	0.9 [+0.1]
Random (mm)	0.7 [-0.5]	1.3 [-1.2]	1.2 [-0.1]

Table 6.1: Mean values of the intrafraction motion errors from McPartlin et al. [20], with the difference compared to the values computed in this work in brackets.

can be explained by the quite little time between the installation of the patient on the treatment couch and the first imaging. The patient may therefore not have the time to relax and adopt its definitive position, leading in a shift of the target in the first minutes after the first CBCT. This global movement certainly also affects the margin, as in the errors, both random and systematic, not only the real intrafraction motion will be taken into account, but also the variation in the magnitude of the relaxation of the patient. This last effect is a parasitic data, as it is expected to be observed only in the first minutes after the installation of the patient, and not during the actual treatment, which starts at least 15 minutes later. It should therefore be kept in mind that the margin computed with these values is probably overestimated.

The last thing to consider in the intrafraction motion is the measurement error. Thanks to the help of a physician, I was able to estimate the standard deviation of the error made in the matching of the prostates in the CBCT. The obtained values were : $0.3mm$, $0.6mm$ and $0.4mm$ for the LR, AP and CC directions, respectively. These errors may seem relatively big compared to the means, but are still actually low for an inter-observer matching deviation. It is also acceptable for clinic purpose, considering that the margin used in clinical routine rarely has a precision of more than $1mm$.

6.4 Delineation

The computation of the delineation uncertainty is the most complex part of this work. Indeed, the delineation uncertainty has always been considered as fully systematic, but in adaptive radiotherapy, the original CTV delineated on the CT-sim is always modified before each fraction, at least by the AI, and very often by the physician too. It is therefore clearly not fully systematic anymore. It is not, however, fully random either, since the original CTV used as a reference is already prone to

some errors in a certain extent. In fact, the CTV delineated on the CT-sim will most likely propagate its own delineation uncertainties when deformed during the adaptive workflow. Those might be partially erased during the manual edition of the CTV's contours by the physician during the plan adaptation. Still a bias subsists as the reference, in the absence of contrast agent and correctly matched MRI, would be the initial CTV contours of the CT-sim. Maximum efforts were put in minimizing the initial delineation uncertainty on the CTV, which is by definition the whole prostate, e.g. a well defined organ. This latter was delineated by a physician specialized in prostate treatment, using a reference CT-sim with both bowel and bladder opacification using contrast agent and an MRI. The base of the bladder was used as a fixed point in space to match the MRI and the CT-sim over the prostatic area. Then the prostate was delineated on the MRI and propagated and adjusted in right-left for the levator ani on the CT-sim.

This part is also the one where the biggest assumptions have been made. As a reminder, we considered that the prostate motions were only represented by translations, that its shape doesn't change, and that the delineations done by the physicians on the CT-sim with the help of an MRI are correct. These are quite strong hypotheses, that will be justified in this section.

The rotations of the prostate has been quantified by many studies, with values, for inter-fractions variations, of 2° to 4° on average, according to Van Herk et al. [12], or more recently Graf et al. [21]. Thanks to the nearly spherical shape of the prostate, these relatively small rotations should not have a significant impact, except maybe in the region of the apex, which is the least spherical part of the prostate, and then the most likely for rotation to impact the delineation uncertainty.

According to Deurloo et al. [22], the variations of the shape of the prostate is small compared to the intra-observer variability. The largest variations have been observed in the anterior and posterior parts of the prostate, with $0.8mm$ and $0.9mm$ of averaged variations, respectively. Propagated to the total margin, this correction reduce the margin by $0.13mm$ and $0.17mm$ in the anterior and posterior directions, respectively. For the other parts, the variations are smaller, or even unmeasurable, due to much larger intra-observer variability. This contribution can therefore clearly be neglected. The shape correction only contributes to a reduction of the total margin, since it is taken into account in the delineation uncertainty computation, despite being corrected by the system during the adaptation. The shape variation should therefore be removed from the computed delineation uncertainty to find the true

error.

Finally, the assumption that the average delineation for one patient is correct may be expressed in another way. Actually, the systematic delineation uncertainty is defined as the standard deviation of the mean delineation difference between a reference, the delineation from the CT-sim, and the delineations from the CBCT of every fraction. Even if the average delineation may not be perfect, the standard deviations of the mean difference should still be a good estimator of the systematic error, thanks to the difference of delineation techniques between the CT-sim and the CBCTs. Indeed, the reference delineation is realised with the help of a MRI, that allows for a better precision than tomography. We can therefore consider that the error on the reference image is relatively small, and nearly independent of the ones made at every fraction. There will still be a remaining systematic error on the reference delineation, of course, but without in situ data of the prostate, one could only approach the ground truth by realising a study implying several physicians, delineating the same prostates on several patients, but this kind of studies are out of the scope of this work, and a potential systematic error due to anatomy ambiguities would still not be taken into account anyway. The method we have chosen is therefore, in our opinion, the most effective we could use, given the information and resources available. For the random contribution, as it only uses the standard deviations of the variations, the delineation random error is completely independent of a potential error in the reference delineation, this assumption is therefore unnecessary for its computation.

Now for the actual results, as expected, the systematic error is significantly smaller than the isotropic error of $2.5mm$ proposed by Van Herk [23] that was used until now, with values ranging from $0.7mm$ to $1.8mm$. It is also a bit smaller than the $1.7mm$, $2mm$, $2.5mm$ errors for LR, AP and CC directions, respectively, find by Rasch et al. [24]. But this reduction of the systematic margin comes at the price of a new contribution to the random margin that was not present before. The total delineation uncertainty is given in table 6.2, with the random contribution taken into account.

This total error is close enough to what can be found in the literature, with a significant reduction in the posterior and caudal directions compared to the results from Rasch et al. [24]. The low differences observed strengthen the relevance of the assumptions made for this part.

Total delineation uncertainty (mm)					
Left	Right	Anterior	Posterior	Cranial	Caudal
1.7	1.6	1.8	1.3	2.4	1.8

Table 6.2: Total delineation uncertainty in every direction, obtained by computing the quadratic sum of the systematic and random contributions

The slightly larger delineation uncertainty observed in the CC direction can be explained by the lower resolution of the CBCT and CT images in this direction. For the ETHOS system, the slice thickness in the CBCT images is 2mm, the precision of the delineation is therefore limited to 1mm in the CC direction.

Thanks to the fact that the random contributions have a lower impact on the final margin than the systematic ones when computed with the Van Herk margin recipe, the new delineation uncertainty measured in this work allows to reduce significantly the PTV margin for every direction, not only in the posterior and caudal ones, where the total delineation uncertainty is smaller. A comparison of the margins computed with the delineation uncertainties proposed by Van Herk et al. [23], Rasch et al. [24] and from this work is given in table 6.3.

	Total margin (mm)					
	Left	Right	Anterior	Posterior	Cranial	Caudal
This work	4.4	4.3	7.2	6.7	6.3	4.6
Van Herk et al. [23]	7.1	7.1	9.2	9.2	7.2	7.2
Rasch et al. [24]	5.3	5.3	8.3	8.3	7.2	7.2

Table 6.3: Comparison of the total margins computed with different delineation uncertainties

The benefits for the margin are then particularly large for the LR direction, especially compared to the Van Herk et al. delineation uncertainty.

6.5 Total margin

The final margin computed in the previous chapter already shows that a reduction of the PTV margin is justified, especially in the left, right and caudal directions. Nevertheless, some improvements could still be made, as explained in the previous sections. Indeed, the intrafraction error found in the literature seems more in agreement with the real intrafraction motion of the patients in the CUSL radiotherapy workflow. Furthermore, the shape variation, although small, should be taken into account to make the margin more relevant. Finally, given the fact that a large part of the final margin is due to 1 or 2 outliers, considering the margin without the patient with the most extreme values may be interesting.

A few different margins have therefore been computed and compared with the final margin in figure 6.1. The first one is the literature margin, computed with the intrafraction motion from McPartlin et al. [20] and delineation errors from Rasch et al. [24]. This margin is a bit higher but very similar to the final margin (less than $1mm$ higher on average), except for the caudal direction, where there is a $2.7mm$ difference. This relatively low difference between the two margin is explained by the compensation of the smaller intrafraction motion error by the larger delineation uncertainty found in the literature, compared to the values computed in this work.

The second margin computed is the margin without outlier. This margin is the same as the final margin, but the first patient, who had by far the biggest intrafraction motion (differs by more than 2 standard deviations from the mean for the LR and AP directions), was removed from the study. The resulting margin is significantly lower in the AP direction, with reductions of $1.3mm$ and $1.6mm$ in the anterior and posterior directions respectively, and slightly lower in the left, right and caudal directions.

Finally, the third margin is computed with what I though was the most relevant data. It uses the literature intrafraction motion error from McPartlin et al. [20], the delineation uncertainty found in this work on which a correction was applied to remove the contribution of the shape variation in the anterior and posterior directions. An outlier was also removed from the delineation uncertainty data, but since the variability of the measures are lower for the delineation than for the intrafraction error, this removal has only a minor effect, mostly visible in the anterior direction, where the margin drops from $4.5mm$ to $3.9mm$. This last margin is interesting, because it suggests that a margin of $4mm$ in the left, right, anterior and posterior

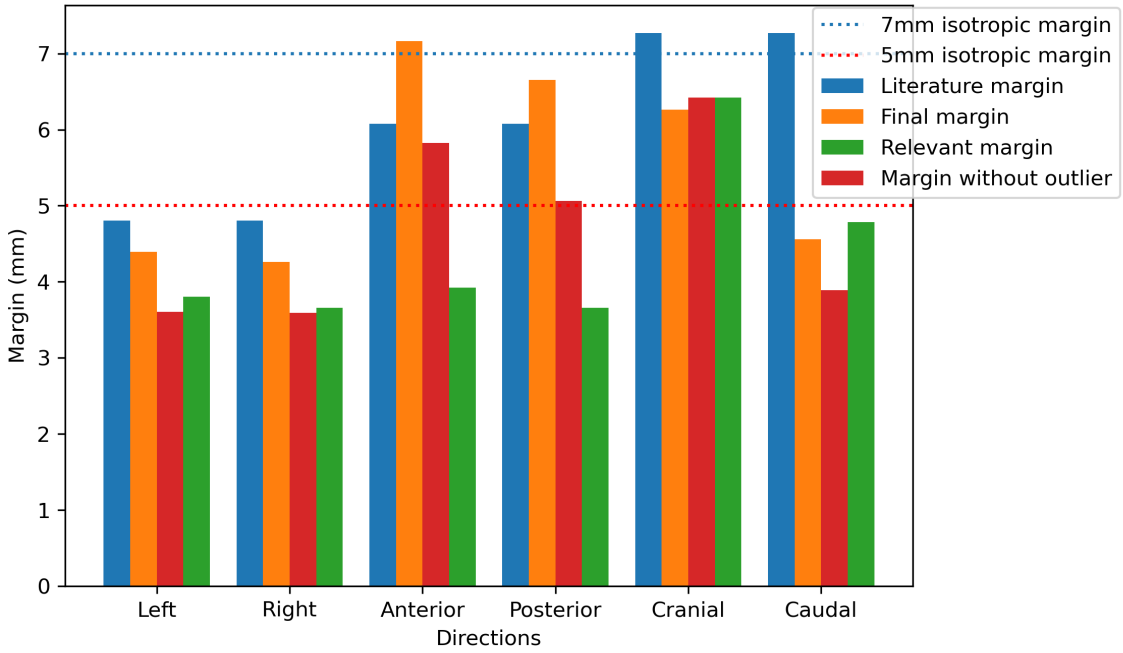

Figure 6.1: Comparison of the margins computed using different data. All margins share the same penumbra and setup error, the differences come only from the delineation and intrafraction motion errors. The Literature margin is computed using the intrafraction motion and delineation errors found in the literature. The final margin is computed with all the results of this work. The margin without outlier is the same as the final margin, from which the data of the most outlier patient have been removed. Finally, the relevant margin is the margin computed with the literature intrafraction error and the delineation uncertainty found in this work, corrected for the prostate shape variation and without the outlier.

directions is sufficient, combined with a $5mm$ caudal and a $6mm$ to $7mm$ cranial margins. This result is close to what many recent works are showing, that a $5mm$ isotropic margin is sufficient for the IGRT of the prostate cancer.

6.6 Limitations

6.6.1 Limitations to the Van Herk margin recipe

In order to derive a margin recipe easy to use in clinical routine, Van Herk et al. made some assumptions that must be justified and that possibly restrain the use of the recipe to a given range of tumors and configurations.

The development is made for a spherical CTV, and can be easily generalized for ellipsoids by separating the integral for every direction. A consequence of considering a spherical CTV is that the rotations have no impact, and are therefore not taken into account. As explained in the previous section, the approximation is good for the prostate, since it is a nearly spherical shaped organ, and its usual rotations are small [12][21], but for other targets, this approximation may make the Van Herk margin recipe unsuitable.

The mathematical development is only correct in the central limit theorem approximation, which requires to have a relatively large amount of random variables summed up together in order to obtain a nearly normal distribution for the total error. In this case, there are only 3 contributions for both the systematic and the random margins, with sometimes one contribution largely dominating the others. Without other information, it is therefore clear that the central limit theorem conditions are not fulfilled. Actually, the individual errors considered are already nearly normally distributed, as they are usually the result of numerous smaller contributions, their sum therefore follows a normal distribution even if there are only few of them. The only contribution that may significantly differ from a normal distribution is the organ motion, especially for tumors influenced by the respiratory movement. Before using the Van Herk margin recipe, it is therefore essential to check that the organ motion, which is also implied in the intrafraction motion, is not dominant. In the case of the adaptive radiotherapy of prostate cancer, the inter-fraction organ motion is not considered, as it is corrected by the adaptation, and its intrafraction contribution will be summed up with a lot of other random errors, so by the central

limit theorem, we can consider the total error as normally distributed.

The last assumption is that there are an infinite number of fractions. This approximation allows not to consider the random error to compute the systematic margin. A correction can be done for low fractionation treatments, like stereotactic radiotherapy, by quadratically adding to the systematic contributions the total random contribution divided by the square root of the number of fractions, and removing the same contribution to the random margin. For the treatments that interest us, with at least 20 fractions, the approximation is reasonable, and applying a correction would only add $0.2mm$ in the posterior direction, where the random margin is the largest, and therefore the correction is the most important.

6.6.2 Specific limitations to this computation method

The patients considered in this study where among the first to be treated using adaptive radiotherapy by the staff of the CUSL. The variability and the time needed to realise the different steps may therefore decrease in the coming years, thanks to a gain of expertise from the staff involved in the treatment process.

With only 10 patients, the statistical variability may be important. By making subsets of 9 patients and computing the margin for all of them, we find that the margin varies from -15% to +5% on average. This variation is indeed quite important, more than twice the standard deviation of the measurement error, and is mostly due to very important intrafraction motions from 1 or 2 patients. Adding patients to the study would therefore really improves the quality of the results. It may also reduce the global margin, as there is a clear diminution of the intrafraction motion between the first patients, treated in August and September 2021 and the most recent ones, when the staff had already a few months of experience, probably due to quicker procedures and maybe better patient supervision. As this statistical variability mostly affects the intrafraction motion error, and not the delineation uncertainty, it is only impacting the final margin presented in chapter 5, and not the more relevant margin suggested at the end of section 6.5.

The majority of the assumptions, errors and uncertainties listed in this chapter are not expected to counterbalance each other. Most of them are more likely to add up in one direction, which would lead to an overestimation of the margin.

As explained in section 4.2, the method to compute the delineation uncertainty involves projecting the contours of the prostates onto a unit sphere. This process is only possible if the polar and azimuthal coordinates of every point of the contour are unique. Otherwise, when projected onto the sphere, some parts of the contour may superimposed, and a single projected point may be associated with several different radial distances, which would induce errors in the computation. It is not an issue for contours with convex or nearly-convex shapes, as the prostate, but it would be if the method was used on more complex elements.

The ultimate goal of the computation of new margins for adaptive radiotherapy was not only to ensure the dose coverage of the CTV despite the geometrical errors, but also and mostly to reduce the dose to the organs at risk, and therefore the risk of unwanted side-effects. The most radiosensitive organs in the pelvic region are the rectum and the bladder, which are mostly situated in the posterior and cranial directions, respectively. If we compare the relevant margin (see figure 6.1) with the previously used isotropic 7mm margin, one can notice that there is an important gain in the posterior direction, but it is not the case in the cranial direction, mostly due to a higher delineation uncertainty for that part. A significant reduction of toxicity is therefore expected in the rectum, but not in the bladder.

6.7 Perspectives

Many improvements may be done to this work in order to improve the results, confirm the clinical benefits and generalise the workflow for other tumor types and localizations.

As mentioned earlier, the statistical variability is still relatively large, due to the low number of patients integrated to the study. As of today, more than 15 other prostate cancers have been treated using adaptive radiotherapy in the CUSL. Those data could be added to the study in order to reduce this statistical variability. Data from other centers using the ETHOS system could also be considered to compute a more generalized margin, that would not be specific to the CUSL radiotherapy department.

It would also be interesting to make the same kind of work for the seminal vesicles, as they are almost always treated at the same time as the prostate. Some changes

on the procedure should therefore be made, as some assumptions would no longer be valid. The absence of rotations, for example, which is used in the computation of the delineation and the intrafraction motion errors, is not true at all for the seminal vesicles. Indeed, they have a much more oblong shape than the prostate, and tend to rotate in the transverse plane depending on the filling of the rectum and the bladder. The potential error associated with the rotation could therefore be large. Furthermore, the shape of the seminal vesicles may change a lot during the treatment, as it is not a rigid mass like the prostate, and the global shape is not always convex. For these two reasons, the Python code for the delineation uncertainty (see appendix A), in its current form, would not provide reliable results.

In addition to the seminal vesicles, this work could also be adapted to other kind and tumor locations, with a lot of caution. Indeed, as explained above, the assumptions made limit the range of tumors for which the computation can be easily transposed. In general, it should be kept in mind that this method and the codes developed are limited to convex-shaped tumors, with negligible rotations and shape changes.

The ETHOS emulator, that allows to simulate treatments with the exact same workflow as on the ETHOS system, should be used to compare treatments that use the ancient PTV margin with treatments that use the new one, to see if there are actual benefits in term of dose to the organs at risk.

As mentioned in chapter 3, the prostate cancer has the particularity that the CTV is defined as the entire prostate volume, and not as the volume of identifiable tumors eventually increased by a margin to cover the micro extensions, like it is for the vast majority of the other cancers. This is caused by the difficulty of seeing the actual tumors inside the prostate volume on medical images. Still, the prostate cancer comes in the form of well defined tumors inside the prostate, that can be identified through IRM or biopsies. Irradiating the entire prostate volume can therefore already be considered as taking a security margin. With this idea in mind, many studies have been made to improve the treatment of prostate cancer by focusing on the real position and distribution of the tumors. Ou et al. [25] realised a prostate biopsy based atlas of the tumor presence probability. This atlas is then a 3D representation of the prostate, where each voxel is given the probability of the presence of cancerous tissues. That probability map can then be used to reduce the PTV margin, by considering it as a negative systematic error with a given standard deviation. This approach has not yet been implemented in clinical routine, but it

should allow a drastic reduction of the PTV margin in the anterior direction, since the tumors seems, given the early results, to be mostly concentrated into the posterior part of the prostate gland.

Chapter 7

Conclusion

A method was developed to compute custom adaptive radiotherapy PTV margin that is implementable in clinical routine and easily adjustable according to the protocols and staff training of a specific department. This method allows to take advantage of the particularities of the adaptive radiotherapy workflow, and specifically, to consider separately the random and the systematic contributions of the delineation uncertainty.

The application of this method to the particular case of the treatment of prostate cancers in the radiotherapy department of the CUSL shows that the separation of the previously fully systematic delineation uncertainty into random and systematic contributions has a major impact on the total PTV margin. That reduces it to 3.8, 3.7, 3.9, 3.7, 6.4 and 4.8mm in the left, right, anterior, posterior, cranial and caudal directions, respectively, which represents a reduction of 11 to 40% compared with the margin of 4.8, 6.1 and 7.3mm computed with a fully systematic delineation uncertainty of 1.7, 2 and 2.5mm in the LR, AP and CC directions, respectively.

These results justify the reduction of the isotropic PTV margin from the commonly reported 7mm to 5mm, and even suggest that it could be lowered down to 4mm in the left, right, anterior and posterior directions.

Due to the assumptions that have been made through this work, this method is still restricted to the computation of margins for specific types of tumors, like the prostate, which neither rotate nor undergoes a change of shape. But some work could be made to generalize it to almost all kinds of tumors.

Bibliography

[1] Global Cancer Observatory. *World fact sheet*. 2020. URL: https://gco.iarc.fr/today/data/factsheets/populations/900-world-fact-sheets.pdf.

[2] PDQ Prostate Cancer Treatment. Bethesda. MD: National Cancer Institute. *PDQ® Adult Treatment Editorial Board*. URL: https://www.cancer.gov/types/prostate/hp/prostate-treatment-pdq. Updated <02/02/2022>. Accessed <06/04/2022>. [PMID: 26389471].

[3] Serena Gianfaldoni et al. "An overview on radiotherapy: From its history to its current applications in dermatology". In: *Open Access Macedonian Journal of Medical Sciences* 5 (4 Special Issue GlobalDermatology 2017), pp. 521–525. ISSN: 18579655. DOI: 10.3889/oamjms.2017.122.

[4] Varian Medical Systems Inc. *Halcyon and Ethos Radiotherapy System Instructions for Use*. Oct. 2019.

[5] Edmond Sterpin. *WRDTH3160-Computed Dosimetry*. UCLouvain. 2022.

[6] Marcel Van Herk, Peter Remeijer, and Joos V Lebesque. "The probability of correct target dosage: dose-population histograms for deriving treatment margins in radiotherapy". In: *Int. J. Radiation Oncology Biol. Phys.* 47 (4 2000), pp. 1121–1135.

[7] A. Bel, M. van Herk, and J. V. Lebesque. "Target margins for random geometrical treatment uncertainties in conformal radiotherapy". In: *Medical Physics* 23.9 (1996), pp. 1537–1545. DOI: https://doi.org/10.1118/1.597745. eprint: https://aapm.onlinelibrary.wiley.com/doi/pdf/10.1118/1.597745. URL: https://aapm.onlinelibrary.wiley.com/doi/abs/10.1118/1.597745.

[8] Joep C. Stroom et al. "Inclusion of geometrical uncertainties in radiotherapy treatment planning by means of coverage probability". In: *International Journal of Radiation Oncology, Biology, Physics* 43.4 (1999), pp. 905–919. DOI: https://doi.org/10.1016/S0360-3016(98)00468-4.

[9] Marcel Van Herk, P. Remeijer, and J.V. Lebesque. "Inclusion of geometric uncertainties in treatment plan evaluation". In: *International Journal of Radiation Oncology Biology Physics* 52.5 (2002), pp. 1407–1429. DOI: 110.1016/s0360-3016(01)02805-x.

[10] Marcel Van Herk. "Errors and Margins in Radiotherapy". In: *Seminars in Radiation Oncology* 14 (1 2004), pp. 52–64. ISSN: 10534296. DOI: 10.1053/j.semradonc.2003.10.003.

[11] Coen Rasch et al. "Definition of the prostate in CT and MRI: a multi-observer study". In: *International Journal of Radiation Oncology*Biology*Physics* 43.1 (1999), pp. 57–66. ISSN: 0360-3016. DOI: https://doi.org/10.1016/S0360-3016(98)00351-4. URL: https://www.sciencedirect.com/science/article/pii/S0360301698003514.

[12] Marcel Van Herk et al. "Quantification of organ motion during conformal radiotherapy of the prostate by three dimensional image registration". In: *J. Radiation Oncology Biol. Phys* 33 (5 1995), pp. 131–1320.

[13] Sukhdeep K. Gill et al. "Determination of optimal PTV margin for patients receiving CBCT-guided prostate IMRT: Comparative analysis based on CBCT dose calculation with four different margins". In: *Journal of Applied Clinical Medical Physics* 16 (6 2015), pp. 252–262. ISSN: 15269914. DOI: 10.1120/jacmp.v16i6.5691.

[14] Meetakshi Gupta et al. "Effect of imaging frequency on PTV margins and geographical miss during image guided radiation therapy for prostate cancer". In: *Practical Radiation Oncology* 8 (2 Mar. 2018), e41–e47. ISSN: 18798500. DOI: 10.1016/j.prro.2017.09.010.

[15] P. Remeijer et al. "A general methodology for three-dimensional analysis of variation in target volume delineation". In: *Medical Physics* 26 (6 1999), pp. 931–940. ISSN: 00942405. DOI: 10.1118/1.598485.

[16] E Sterpin and D Dechambre. *Calcul de la pénombre pour machine Varian Halcyon afin de déterminer les marges de sécurité de PTV*. 2020.

[17] Falk Pönisch et al. "Properties of unflattened photon beams shaped by a multileaf collimator". In: *Medical Physics* 33 (6 2006), pp. 1738–1746. ISSN: 00942405. DOI: 10.1118/1.2201149.

[18] Essa Mayyas et al. "Evaluation of multiple image-based modalities for image-guided radiation therapy (IGRT) of prostate carcinoma: A prospective study". In: *Medical Physics* 40 (4 2013), p. 41707. DOI: https://doi.org/10.1118/1.4794502. URL: https://aapm.onlinelibrary.wiley.com/doi/abs/10.1118/1.4794502.

[19] Harun Badakhshi et al. "Image-guided Radiotherapy with Implanted Markers and Kilovoltage Imaging and 6-dimensional Position Corrections for Intrafractional Motion of the Prostate". In: *Anticancer Research* 33 (Sept. 2013). ISSN: 4117-4122.

[20] A. J. McPartlin et al. "MRI-guided prostate adaptive radiotherapy – A systematic review". In: *Radiotherapy and Oncology* 119 (3 June 2016), pp. 371–380. ISSN: 18790887. DOI: 10.1016/j.radonc.2016.04.014.

[21] Reinhold Graf et al. "Interfraction rotation of the prostate as evaluated by kilovoltage X-ray fiducial marker imaging in intensity-modulated radiotherapy of localized prostate cancer". In: *Medical Dosimetry* 37 (4 2012), pp. 396–400. ISSN: 09583947. DOI: 10.1016/j.meddos.2012.02.006.

[22] Kirsten E.I. Deurloo et al. "Quantification of shape variation of prostate and seminal vesicles during external beam radiotherapy". In: *International Journal of Radiation Oncology Biology Physics* 61 (1 Jan. 2005), pp. 228–238. ISSN: 03603016. DOI: 10.1016/j.ijrobp.2004.09.023.

[23] Marcel Van Herk. *Margins and margin recipes*. 2011.

[24] Coen Rasch, Roel Steenbakkers, and Marcel Van Herk. "Target definition in prostate, head, and neck". In: *Seminars in Radiation Oncology* 15 (3 2005), pp. 136–145. ISSN: 10534296. DOI: 10.1016/j.semradonc.2005.01.005.

[25] Yangming Ou et al. "Sampling the spatial patterns of cancer: Optimized biopsy procedures for estimating prostate cancer volume and Gleason Score". In: *Medical Image Analysis* 13 (4 Aug. 2009), pp. 609–620. ISSN: 13618415. DOI: 10.1016/j.media.2009.05.002.

Appendix A

delineation uncertainty code

```
import pydicom
import numpy as np
from scipy.interpolate import LinearNDInterpolator
from scipy.spatial import ConvexHull


#Extract the coordinates of the points of a contour and store them into an array

def extract_point(contour):
  array = []
  for sli in contour:
    pxl = sli.ContourData._list

    for i in range(0, len(pxl), 3):
      array.append([pxl[i], pxl[i + 1], pxl[i + 2]])

  array = np.array(array)
  return array

#Switch to spherical coordinates

def Spherical(xyz):
  ptsnew = np.zeros(xyz.shape)
  xy = xyz[:, 0] ** 2 + xyz[:, 1] ** 2
  ptsnew[:, 0] = np.sqrt(xy + xyz[:, 2] ** 2)
  ptsnew[:, 1] = np.arctan2(np.sqrt(xy), xyz[:, 2])
  ptsnew[:, 2] = np.arctan2(xyz[:, 1], xyz[:, 0]) + np.pi
  return ptsnew
```

```
#Switch to cartesian coordinates

def Cartesian(theta, phi):
  return np.array([
    np.sin(theta) * np.cos(phi),
    np.sin(theta) * np.sin(phi),
    np.cos(theta)])

#Compute the coordinate of the center of an array of points

def get_centroid(array):
  hull = ConvexHull(array)
  cx = np.mean(hull.points[hull.vertices, 0])
  cy = np.mean(hull.points[hull.vertices, 1])
  cz = np.mean(hull.points[hull.vertices, 2])

  return [cx, cy, cz]

#Translate all the points of an array to place the center of mass at the origin

def assign_origin(array, centre):
  array[:, 0] = array[:, 0] - centre[0]
  array[:, 1] = array[:, 1] - centre[1]
  array[:, 2] = array[:, 2] - centre[2]
  return array

#Compute the mean delineation variation in every direction between the
#simulation CT and a given CBCT

def prostate_diff(file, ref_index, cbct_index):
  ds = pydicom.read_file(file)

#Extract the structure sets of the prostate from the reference CT and the
#considered CBCT from the Dicom file and store the coordinates of the points
#into 3D arrays

  ref_ctr = ds.ROIContourSequence[ref_index].ContourSequence
  cbct_ctr = ds.ROIContourSequence[cbct_index].ContourSequence

  points = extract_point(ref_ctr)
```

```
    points_cbct = extract_point(cbct_ctr)

    xx, yy, zz = np.mgrid[-1:1:100j, -1:1:100j, -1:1:100j]

#For every sets of points, compute the center of mass and center the structure

    centroid = get_centroid(points)
    centroid_cbct = get_centroid(points_cbct)

    points = assign_origin(points, centroid)
    points_cbct = assign_origin(points_cbct, centroid_cbct)

    spherical_points = points.copy()
    spherical_points_cbct = points_cbct.copy()

#Project the points onto a unit sphere while assigning their radial distance
#as a parameter

    spherical_points = Spherical(spherical_points)
    spherical_points_cbct = Spherical(spherical_points_cbct)

    Cartesian_points = Cartesian(spherical_points[:, 1], spherical_points[:, 2]).T
    Cartesian_points_cbct = Cartesian(spherical_points_cbct[:, 1],
                    spherical_points_cbct[:, 2]).T

#Interpolate the radial distance into a regular mesh to be able to compare the
#two sets of values

    Interp = LinearNDInterpolator(Cartesian_points, spherical_points[:, 0])

    Interp_cbct = LinearNDInterpolator(Cartesian_points_cbct,
                      spherical_points_cbct[:, 0])

    Points_in_mesh = Interp(xx, yy, zz)
    Points_in_mesh_cbct = Interp_cbct(xx, yy, zz)

#Compute the difference for every coordinates in the regular mesh and sort the
#values according to their positions

    Difference_map = Points_in_mesh_cbct - Points_in_mesh
    Difference_map_clean = np.array([0, 0, 0, 0])
```

```
sum_left = sum_right = sum_ant = sum_pos = sum_head = sum_foot = 0
n_left = n_right = n_ant = n_pos = n_head = n_foot = 0

for i in range(Difference_map.shape[0]):
  for j in range(Difference_map.shape[1]):
    for k in range(Difference_map.shape[2]):
      if not np.isnan(Difference_map[i, j, k]):
        if np.isnan(Difference_map[i + 1, j, k]) or \
            np.isnan(Difference_map[i - 1, j, k]) or \
            np.isnan(Difference_map[i, j + 1, k]) or \
            np.isnan(Difference_map[i, j - 1, k]) or \
            np.isnan(Difference_map[i, j, k + 1]) or \
            np.isnan(Difference_map[i, j, k - 1]):
          Difference_map_clean = np.vstack((Difference_map_clean,
                    [Difference_map[i, j, k], i, j, k]))
          x = i-50
          y = k-50
          z = j-50
          if np.abs(np.arcsin(z/np.sqrt(x**2+y**2+z**2)))<np.pi/4:
            if x>0 and np.abs(np.arctan(y/x))<np.pi/4:
              sum_right += Difference_map[i, j, k]
              n_right += 1
            if x<0 and np.abs(np.arctan(y/(-x)))<np.pi/4:
              sum_left += Difference_map[i, j, k]
              n_left += 1
            if y>0 and np.abs(np.arctan(x/y))<np.pi/4:
              sum_head += Difference_map[i, j, k]
              n_head += 1
            if y<0 and np.abs(np.arctan(x/(-y)))<np.pi/4:
              sum_foot += Difference_map[i, j, k]
              n_foot += 1
          elif z<0:
              sum_ant += Difference_map[i, j, k]
              n_ant += 1
          elif z>0:
              sum_pos += Difference_map[i, j, k]
              n_pos += 1

Difference_map_clean = np.delete(Difference_map_clean, 0, axis=0)
```

```
#Compute the mean difference for every direction

  Mean_left = sum_left / n_left
  Mean_right = sum_right / n_right
  Mean_ant = sum_ant / n_ant
  Mean_pos = sum_pos / n_pos
  Mean_head = sum_head / n_head
  Mean_foot = sum_foot / n_foot
  print(n_right, n_left, n_head, n_foot, n_ant, n_pos)

  return np.array([[Mean_left, Mean_right, Mean_ant, Mean_pos, Mean_head,
          Mean_foot]])



file = "" #Fill with RTSTRUCT file
ds = pydicom.read_file(file)

#The indexes of the structures can be found in ds -> StructureSetROISequence

ref_index =   #Fill with reference CTV structure index
CBCT_first_index =   #Fill with the first CBCT CTV structure index
CBCT_last_index =   #Fill with the last CBCT CTV structure index
Patient = np.zeros([CBCT_last_index - CBCT_first_index + 1, 6])
for i in range(CBCT_first_index, CBCT_last_index + 1):
  Session = prostate_diff(file, ref_index, i)
  Patient[i - CBCT_first_index, :] = Session
  print(i)

#Compute the global Mean and Standard deviation for the patient

Means = np.mean(Patient, axis=0, keepdims=True)
StdDev = np.std(Patient, axis=0, keepdims=True)
```

Appendix B

Dose fit code

```
import matplotlib.pyplot as plt
import numpy as np
from scipy.optimize import curve_fit

#Compute a zero-centered parable of parameters a and b

def parabole(xdata, a, b):
  return 100 - a * xdata**2 + b*xdata

#Compute a zero-centered gaussian function of standard deviation sigma

def gaussian(xdata, sigma):
  return (1/(sigma*np.sqrt(2*np.pi)))*np.exp(-(xdata ** 2 / (2.0 * sigma ** 2)))

#Compute the convolution of a zero-centered parable of parameters a and b
#truncated to a given width and a gaussian function of standard deviation sigma

def convolution(xdata, a, b, width, sigma1, sigma2):
  cond = (np.abs(xdata) < width).astype(int)
  convol = np.convolve(parabole(xdata, a, b) * cond, gaussian(xdata, sigma1), 'same'
  convol = 100 * convol / max(convol)
  convol = np.convolve(convol, gaussian(xdata, sigma2), 'same')
  convol = 100 * convol / max(convol)
  return convol

#Load the measured dose distribution from a csv file, normalize it and store
#it into an array

Dose_profile = np.loadtxt(open('DoseProfile_10x10_DSP90_Y.csv'),
```

```
            delimiter='\t').T
Dose_profile[1] = 100*Dose_profile[1]/np.amax(Dose_profile[1])
Dose_profile[0] = Dose_profile[0] - Dose_profile[0, np.argmax(Dose_profile[1])]

#Crop the dose profile to remove the lowest values

Cropped_Dose_Profile = np.zeros([2, Dose_profile[0][(Dose_profile[1] > 30)].size])
Cropped_Dose_Profile[0] = Dose_profile[0][(Dose_profile[1] > 30)]
Cropped_Dose_Profile[1] = Dose_profile[1][(Dose_profile[1] > 30)]

#Fit the measured distribution withe the convolution defined above

popt, pcov = curve_fit(convolution, Cropped_Dose_Profile[0], Cropped_Dose_Profile[1],
            bounds=([0, 0, 4.9, 0, 0], [np.inf, 0.001, 5.1, 5, np.inf]))
print(popt)
Dose_fit = convolution(Dose_profile[0], *popt)
Dose_fit = np.roll(Dose_fit, np.argmax(Dose_profile[1]) - np.argmax(Dose_fit))

#Plot the measured and computed dose distributions to check the matching

fig = plt.figure(dpi=200)
plt.plot(Dose_profile[0], Dose_profile[1], label='Measured dose')
plt.xlabel('Distance (cm)')
plt.ylabel('Dose (% of maximum)')
plt.plot(Dose_profile[0], Dose_fit, label='Ideal dose')
plt.legend()
plt.savefig('Figures/Dose_Profile.png', dpi=200)
```

UNIVERSITÉ CATHOLIQUE DE LOUVAIN
Faculté des sciences
Place des Sciences, 2 bte L6.06.01, 1348 Louvain-la-Neuve, Belgique | www.uclouvain.be/sc